The Bioburden and Ionic Composition of Hypersaline Lake Ices: Novel Habitats on Earth and Their Astrobiological Implications

Jacob Buffo[1,1,1], E K Brown[2,2,2], A Pontefract[3,3,3], B E Schmidt[4,4,4], B Klempay[5,5,5], J Lawrence[2,2,2], J Bowman[6,6,6], M Grantham[2,2,2], J B Glass[2,2,2], T Plattner[2,2,2], C Chivers[2,2,2], and Peter Doran[7,7,7]

[1]Dartmouth College
[2]Georgia Institute of Technology
[3]Georgetown University
[4]Cornell University
[5]UCSD
[6]Scripps
[7]Louisiana State University

November 30, 2022

Abstract

We present thermophysical, biological, and chemical observations of ice and brine samples from five compositionally diverse hypersaline lakes in British Columbia's interior plateau. Possessing a spectrum of magnesium, sodium, sulfate, carbonate and chloride salts, these low-temperature high-salinity lakes are analogs for planetary ice-brine environments, including the ice shells of Europa and Enceladus, and ice-brine systems on Mars. As such, understanding the thermodynamics and biogeochemistry of these systems can provide insight into the evolution, habitability, and detectability of high priority astrobiology targets. We show that biomass is typically concentrated in a layer near the base of the ice cover, but that chemical and biological impurities are present throughout the ice. Coupling bioburden, ionic concentration and seasonal temperature measurements, we demonstrate that impurity entrainment in the ice is directly correlated to ice formation rate and parent fluid composition. We highlight unique phenomena including brine supercooling, salt hydrate precipitation, and internal brine layers in the ice cover, important processes to consider for planetary ice-brine environments. These systems can be leveraged to constrain the distribution, longevity, and habitability of low-temperature solar system brines – relevant to interpreting spacecraft data and planning future missions in the lens of both planetary exploration and planetary protection.

The Bioburden and Ionic Composition of Hypersaline Lake Ices: Novel Habitats on Earth and Their Astrobiological Implications

J. J. Buffo[1]*, E. K. Brown[2], A. Pontefract[3], B. E. Schmidt[2], B. Klempay[4], J. Lawrence[2], J. Bowman[4], M. Grantham[2], J. B. Glass[2], T. Plattner[2], C. Chivers[2], P. Doran[5] and the OAST Team

[1] – Dartmouth College
[2] – Georgia Institute of Technology
[3] – Georgetown University
[4] – Scripps Institution of Oceanography
[5] – Louisiana State University
* – Corresponding Author

Keywords: Brines, Ices, Planetary Analogs, Ice-Ocean Worlds, Mars, Halophilic Psychrophiles

Abstract

We present thermophysical, biological, and chemical observations of ice and brine samples from five compositionally diverse hypersaline lakes in British Columbia's interior plateau. Possessing a spectrum of magnesium, sodium, sulfate, carbonate and chloride salts, these low-temperature high-salinity lakes are analogs for planetary ice-brine environments, including the ice shells of Europa and Enceladus, and ice-brine systems on Mars. As such, understanding the thermodynamics and biogeochemistry of these systems can provide insight into the evolution, habitability, and detectability of high priority astrobiology targets. We show that biomass is typically concentrated in a layer near the base of the ice cover, but that chemical and biological impurities are present throughout the ice. Coupling bioburden, ionic concentration, and seasonal temperature measurements, we demonstrate that impurity entrainment in the ice is directly correlated to ice formation rate and parent fluid composition. We highlight unique phenomena including brine supercooling, salt hydrate precipitation, and internal brine layers in the ice cover; important processes to consider for planetary ice-brine environments. These systems can be leveraged to constrain the distribution, longevity, and habitability of low-temperature solar system brines – relevant to interpreting spacecraft data and planning future missions in the lens of both planetary exploration and planetary protection.

1. Introduction

1.1 *Field Site Overview*

The Interior Plateau of central British Columbia houses a diverse array of endorheic (closed basin) hypersaline lakes. Seasonal snowmelt and groundwater flow leaches metals and minerals from the local geology before collecting in the low-lying perennial and ephemeral lakes and playas, where the leachate concentrates and forms salts. The hot and arid summer climate of the region leads to substantial evaporation, and with minimal rainfall to refresh the lakes their salinities dramatically increase, reaching concentrations of 30-40% salt by weight. In some cases, the lakes reach their saturation point and pure hydrated salts (e.g. epsomite, mirabilite, meridianiite, natron, trona) begin to precipitate in the lake waters and underlying sediments [*Renaut and Long*, 1989]. This cyclic concentrative process can lead to the formation of thick (~5m), solid salt basements and columns beneath the lakes [*Jenkins*, 1918; *Renaut and Long*, 1989] (See Figure 1). Many lakes in this region exhibit a unique 'spotted' morphology, where tens to hundreds of individual brine pools subdivide the lake (Figure 1). The formation process of the individual brine pools is currently unknown. Proposed formation mechanisms include density driven subsistence caused by annual salt precipitation [*Renaut and Long*, 1989], bottom up dendritic growth of sub-pool salt structures from the salt basement [*Jenkins*, 1918], and freeze-thaw processes in the shallow subsurface [*Renaut and Long*, 1989], akin to frost heave driven patterned ground formation [*Peterson and Krantz*, 2008]. Regardless of their origin, the brine pools are stable structures whose perimeters do not vary seasonally and have likely remained relatively unchanged over much longer timescales (~10s to 100s of years) [*Renaut and Long*, 1989].

While these extremely high salinity environments are toxic to many organisms, there exists a rich and unique halophilic ecosystem within each of the lakes [*Pontefract et al.*, 2019; *Pontefract et al.*, 2017]. As autumn ends the resident organisms are subjected to an additional environmental stressor – extreme cold. With mean January temperatures ranging from -9 to -12°C and nighttime lows that can exceed -45°C the lakes form a substantial ice cover [*Brown et al.*, 2020a; *Renaut and Long*, 1989]. The ice that forms from the hypersaline brines of these lakes is highly porous and contains both salts and organisms entrained during ice formation. This process further concentrates

the underlying brine, depressing its freezing point by as much as ~9°C, depending on the composition of the lake [*Buffo et al.*, 2019]. The interstitial brine of the ice (brine contained in unfrozen pockets, channels, and grain boundaries) and the underlying brine reservoir constitute novel extreme environments that support a community of halophilic psychrophiles [*Buffo et al.*, 2019; *Pontefract et al.*, 2019; *Pontefract et al.*, 2017].

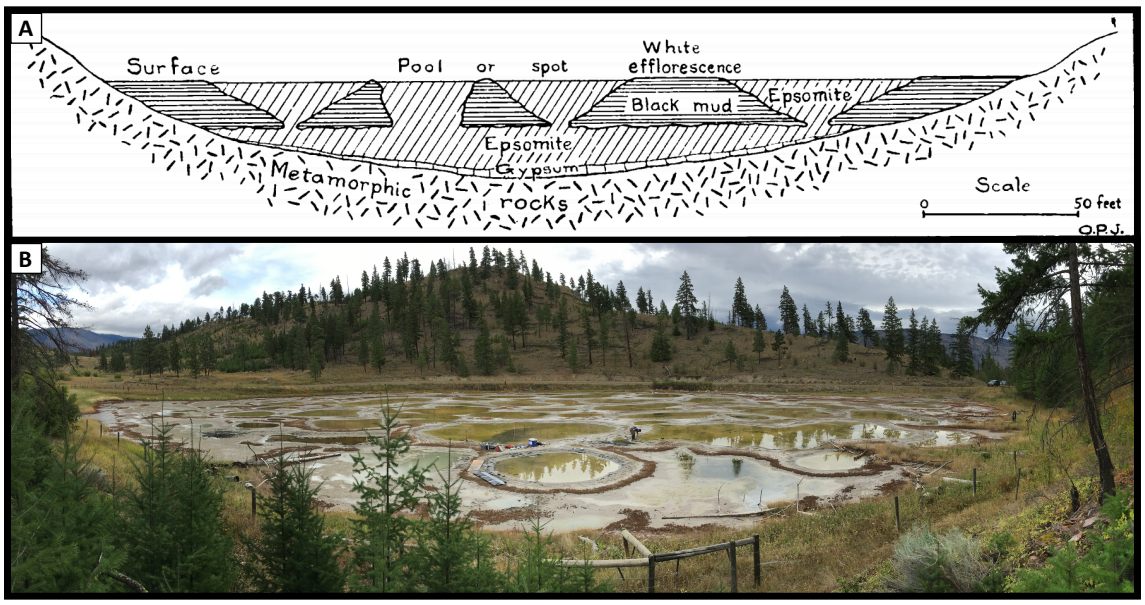

Figure 1: Structure of the hypersaline lakes. A) The subsurface structure of the spotted lakes, depicting the epsomite basement and columns/inverted cones that underly the surficial pools, modified from [*Jenkins*, 1918]. **B)** Photograph of Basque Lake 2, taken in September 2019.

The wintertime abundance and productivity of microfauna in this porous system is likely limited by physicochemical properties of the ice and brine, such as pore connectivity, water activity (A_w; a measure of the thermodynamic availability of water for microbial processes), and chaotropicity/kosmotropicity (a measure of the extent to which solutes disrupt or stabilize biological structures, respectively) [*Loose et al.*, 2011; *Murray et al.*, 2012; *Stevens and Cockell*, 2020; *Weeks and Ackley*, 1986]. The osmotic stress and potentially destabilizing (chaotropic) properties of hypersaline environments is well documented in the literature [*Fisher et al.*, 2021; *Hallsworth et al.*, 2007; *Oren*, 2013] and has even been discussed in the context of Martian environments [*Fox-Powell et al.*, 2016; *Pontefract et al.*, 2017; *Tosca et al.*, 2008]. These works emphasize the importance of the concentration and chemical composition of a brine in governing its habitability, as both A_w and chao-/kosmotropicity (strongly limiting factors for life as we know it [*Fox-Powell and Cockell*, 2018; *Pontefract et al.*, 2017]) are heavily dependent on the ionic species present. In complex multi-component brines, such as these lakes, the competing and combinatory effects of chaotropes and kosmotropes will likely govern the habitability of the system [*Pontefract et al.*, 2019; *Pontefract et al.*, 2017; *Stevens and Cockell*, 2020]. The formation of ice promotes cryoconcentration of the residual brine as salts are efficiently excluded from ice's crystal lattice structure [*Feltham et al.*, 2006; *Hunke et al.*, 2011], eventually saturating the brine and leading to the precipitation of salt hydrates. While low temperatures and brine saturation may limit habitability, both ice and hydrated salts are capable of entraining and preserving biomaterials [*Buffo et al.*, 2019; *Pontefract et al.*, 2017; *Srivastava et al.*, 2021], potentially providing a

mechanism for long term stasis of organisms when conditions become less favorable [*Cosciotti et al.*, 2019; *Srivastava et al.*, 2021].

1.2 *Scientific Motivation*

The most promising worlds within our solar system that may harbor environments suitable for life all lie beyond the sun's habitable zone (e.g., Europa, Enceladus, Mars), precluding the long-term stability of liquid water on their surfaces [*Fox-Powell et al.*, 2016; *Marion et al.*, 2003; *Parkinson et al.*, 2008; *Priscu and Hand*, 2012; *Tosca et al.*, 2008]. As such, most high priority astrobiology targets are situated beneath icy outer shells/regolith or occur as ephemeral/relict surface expressions of subsurface fluids. In the case of Europa and Enceladus this manifests in the form of global ice shells overlying regional or global subsurface oceans [*Čadek et al.*, 2016; *Sotin and Tobie*, 2004], with possible endogenic expression of ocean material through ocean-surface geophysical processes (e.g., diapirism [*Nimmo and Pappalardo*, 2006; *Pappalardo and Barr*, 2004; *Schmidt et al.*, 2011], extensional band formation [*Howell and Pappalardo*, 2018], solid state convection [*Barr and McKinnon*, 2007; *McKinnon*, 1999; *Weller et al.*, 2019], fractures [*Craft et al.*, 2016; *Nathan et al.*, 2019; *Nimmo and Schenk*, 2006; *Walker et al.*, 2014], and plumes [*Bauer et al.*, 2010; *Glein et al.*, 2015; *Sparks et al.*, 2016] – see Figure 2). For Mars it has been suggested that both historical and contemporary shallow subsurface brine systems and episodic surface expression of brine are responsible for the formation of fluvial and lacustrine geomorphological features (e.g., Gale Crater – a potentially remnant analog to the Canadian lake systems investigated here – Figure 2) and continue to interact with and be sourced from observed ground ice [*Carr*, 1987; *Ojha et al.*, *2020; Ojha et al.*, 2015; *Rapin et al.*, 2019; *Toner et al.*, 2014; *Vaniman et al.*, 2004; *Wray et al.*, 2011; *Zorzano et al.*, 2009]. Furthermore, subglacial hydrology in the Noachian era [*Fastook and Head*, 2015; *Ojha et al.*, *2020*] and potential saline lakes beneath the present day south polar layered deposit [*Grau Galofre et al.*, 2020; *Lauro et al.*, 2020; *Orosei et al.*, 2018; *Sori and Bramson*, 2019] may constitute additional habitable aqueous environments, suggesting such systems could have existed in a number of regions in both Mars' past and present. With the unique link between water and life as we know it, identifying and improving our understanding of these ice-ocean/brine systems is imperative to future mission design in the lens of both planetary exploration and planetary protection.

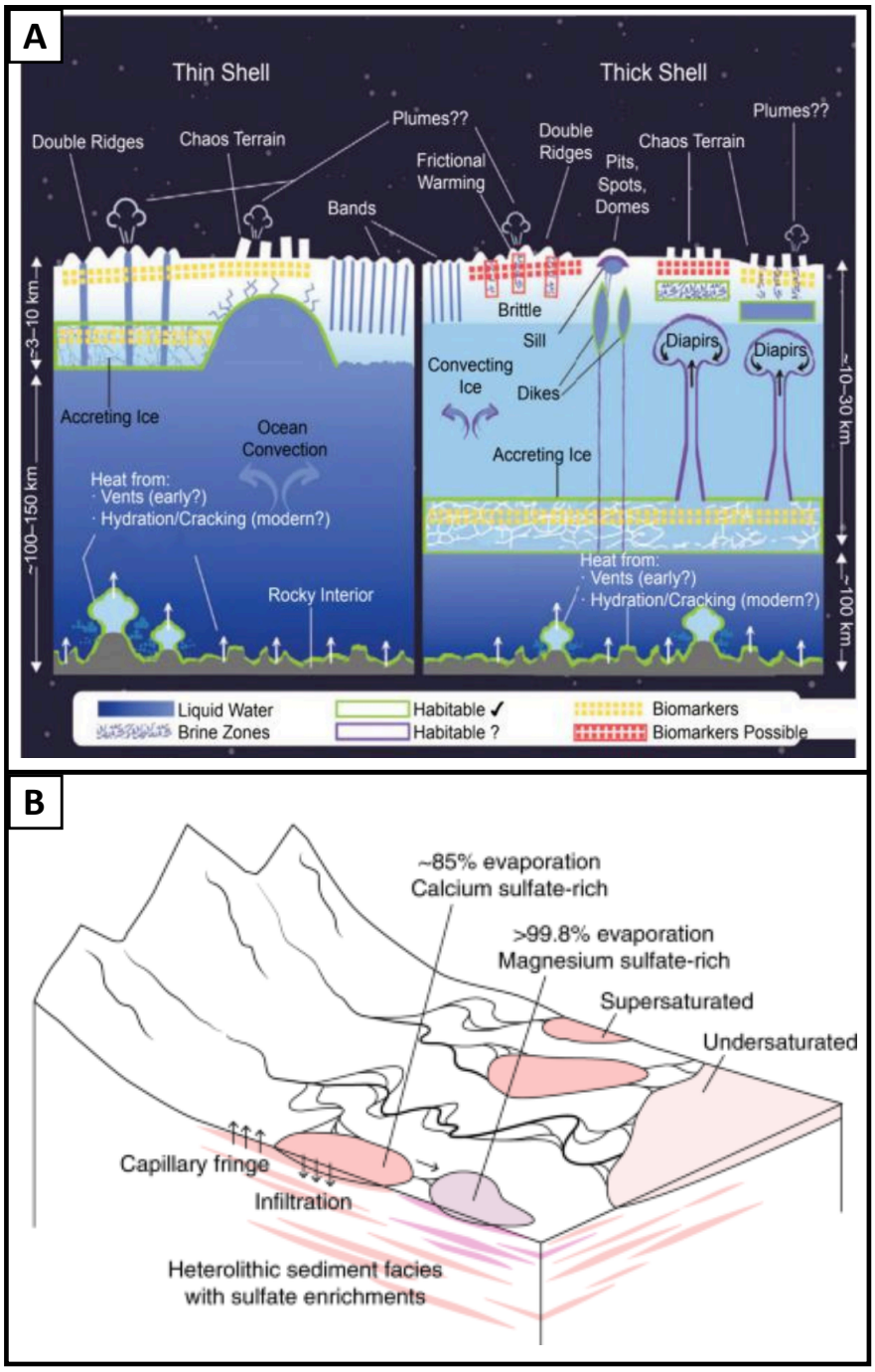

Figure 2 – Putative ice-brine environments on Mars and ice-ocean worlds. A) The ice-ocean-seafloor system of Europa, highlighting the potential for ice shell hydrology driven by regional geodynamics. In addition to the global subsurface ocean, concentrated brine could facilitate stable hydrological feature within the shell. Understanding their biogeochemical evolution is crucial to predicting their distribution, longevity and habitability as well as linking shallow subsurface characteristics to underlying ocean properties. **B)** Predicted fluvial and lacustrine dynamics in Mars' ancient Gale crater [*Rapin et al.*, 2019]. Cyclic filling and evaporation of endorheic pools coupled with freezing surface temperatures could create environments strikingly similar to those found in the Canadian ice-brine systems investigated here (particularly their geochemical evolution and habitability). (Photo Credit: A) [*Schmidt*, 2020] B) [*Rapin et al.*, 2019])

A remaining hurdle exists in accessing and observing the underlying ocean/brine reservoir, as it frequently lies beneath meters or kilometers of ice. In the absence of *in situ* measurements, we rely on remote sensing techniques (e.g., spectrographs, ice penetrating radar) to observe ice characteristics and relate these measurements to properties of the underlying liquid [*Di Paolo et al.*, 2016; *Fanale et al.*, 1999; *Kalousova et al.*, 2017; *Ojha et al.*, 2015; *Orosei et al.*, 2018]. Fortunately, when ice forms it entrains biogeochemical signatures of its parent water reservoir and formation history [*Buffo et al.*, *2020; Buffo et al.*, 2019; *Buffo et al.*, 2018; *Kargel et al.*, 2000]. On Earth, this entrainment has been observed in the salinity and bioburden profiles of both sea ice [*Cottier et al.*, 1999; *Cox and Weeks*, 1974; *Eicken*, 1992; *Loose et al.*, 2011; *Nakawo and Sinha*, 1981; *Thomas and Dieckmann*, 2003] and lake ice [*Murray et al.*, 2012; *Priscu et al.*, 1998; *Santibáñez et al.*, 2019].

While the thermodynamics and biogeochemistry of ice formed from Earth's sodium chloride (NaCl) rich ocean has been studied for nearly a century (e.g., [*Malmgren*, 1927]), the analogous processes in ices formed from more exotic ocean/brine compositions remain less constrained (exceptions being the ice covers of Antarctic dry valley lakes – e.g., [*Doran et al.*, 2003; *Murray et al.*, 2012; *Priscu et al.*, 1998]). Exotic salt assemblages including magnesium, sulfate, and acid-bearing salts have been detected on Europa [*Fanale et al.*, 1999] and magnesium, sulfate, chlorate, and perchlorate salts are ubiquitous components of Mars' geology [*Ojha et al.*, 2015; *Pontefract et al.*, 2017; *Tosca et al.*, 2008; *Vaniman et al.*, 2004]. This is important as it suggests the oceans and brines of other solar system bodies may be quite different than Earth's ocean [*Kargel et al.*, 2000; *Pontefract et al.*, 2017; *Toner et al.*, 2014; *Zolotov*, 2007; *Zolotov and Shock*, 2001]. Likewise, the ice that forms in these planetary environments may have substantially varied characteristics (e.g., microstructure, biochemistry, strength, viscosity). Differing chemistries could drastically impact the habitability and geophysics of ice-ocean/brine worlds on both local and global scales and affect the relationship between ice characteristics and interior reservoir properties and dynamics – an imperative for the interpretation of spacecraft observations.

Fortuitously, the hypersaline lakes of British Columbia provide a natural laboratory in which to observe the thermophysical and biogeochemical evolution of ices formed from compositionally diverse analog brines (e.g., [*Fox-Powell and Cockell*, 2018; *Renaut and Long*, 1989]). Furthermore, the $MgSO_4$ and Na_2SO_4 dominated chemistries of these lakes mirror the predicted ocean/brine compositions of both icy satellites [*Zolotov*, 2007; *Zolotov and Shock*, 2001] and Mars [*Pontefract et al.*, 2017; *Toner et al.*, 2014; *Vaniman et al.*, 2004]. Cumulatively, observations of the thermal, structural, and biogeochemical profiles of British Columbia's diverse hypersaline lakes provide a method to assess the spatiotemporal habitability and biosignature distribution of unique ice-brine analog systems. This not only has far-reaching implications for extremophilic adaptation and the limits of life on Earth but provides an ideal system to investigate the thermophysical evolution and hypothetical biogeochemical dynamics of analogous planetary ice-brine environments while providing a benchmark to validate models designed to simulate these systems (e.g., [*Brown et al.*, 2020b; *Buffo et al.*, 2019; *Buffo et al.*, 2021b]).

2. Methods

Five lakes were visited during two field campaigns (February 2019 and February 2020): Basque Lake 1 [50.60012°, -121.35967°], Basque Lake 2 [50.59336°, -121.34974°], Basque Lake 4 [50.58867°, -121.34317°], Last Chance Lake [51.32775°, -121.63576°], and Salt Lake [51.07298°, -121.58441°] (Figure 3). Basque Lakes 1, 2, and 4 as well as Salt Lake are magnesium

sulfate ($MgSO_4$) dominated systems, while Last Chance Lake is a sodium sulfate (Na_2SO_4) and sodium carbonate (Na_2CO_3) dominated system.

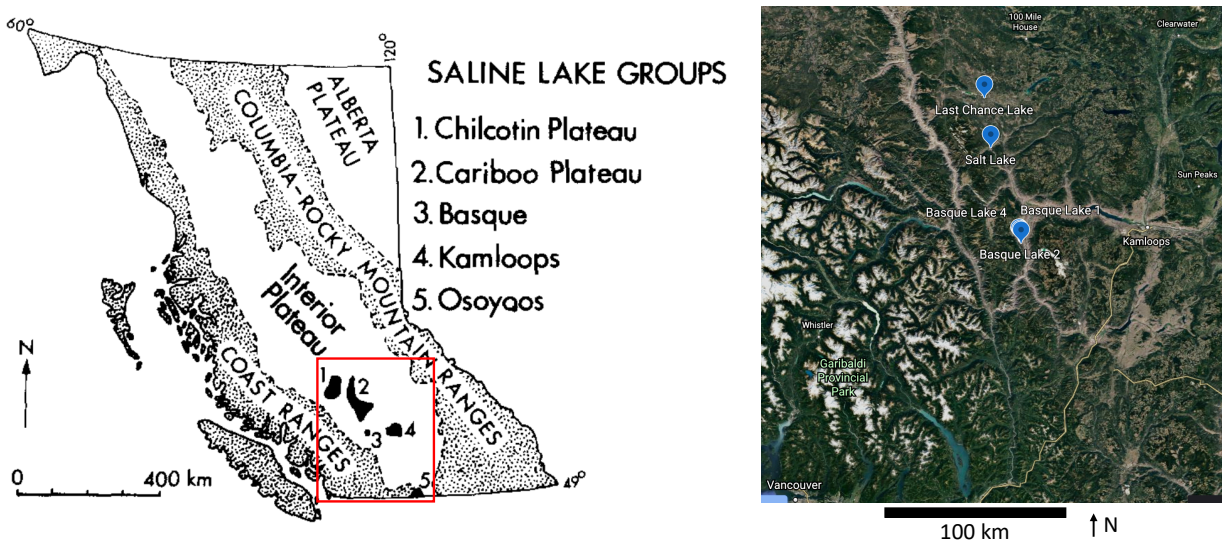

Figure 3 – Hypersaline lake locations. Left) Map of the hypersaline lake groups of central British Columbia (modified from [*Renaut and Long*, 1989]) Last Chance Lake and Salt Lake are members of the Cariboo Plateau group while Basque Lakes 1, 2 and 5 are members of the Basque group. **Right)** Enlarged view of the region outlined in red showing the lake locations visited during February 2020.

At each of the five lakes, sample sites (n=1-3) were selected to represent diverse locations within the lake, either located within discrete brine pools, or as edge to center transects when pools could not be identified due to high lake levels (leading to subaqueous pools). At each site the thickness of the ice and underlying brine layer was measured (Section 3.2). When present, precipitated salt at the base of the brine layer was also measured. Ice cores were extracted from descending sections of the ice column using a carbide tipped 1-1/4" hole saw drill bit (Figure 4c) and stored in sterile amber Nalgene bottles. A temperature profile was taken using a probe thermometer with an accuracy of 0.01 °C as the cores were removed and brine was extracted from the underlying pool/lake using a sterilized syringe if the ice was not frozen to the underlying sediments (Figure 4c and Section 3.3.1). These ice cores and brine samples were used to derive the ionic composition and bioburden profiles of the lake ice-brine systems (Section 3.4). Additionally, long-term temperature loggers that had been deployed in September 2019 to observe seasonal variations in brine and air temperature, were recovered in February 2020 (Section 3.3.2). The HOBO temperature loggers recorded data hourly and were placed at Basque Lake 2 and Last Chance Lake, with one logger positioned directly above the sediment layer in a chosen pool, another in the middle of the water column, and a third logger placed around the lake to gather surrounding air temperature. Finally, brine infill experiments were conducted to assess ice permeability. To do this, 'sackholes' were drilled to different depths within the ice cover and allowed to fill with brine via percolation through the underlying porous ice. By measuring the rate at which the brine infills the hole, the permeability of the ice beneath the hole can be estimated (Section 3.5) [*Freitag and Eicken*, 2003].

Figure 4 – Field work at Basque Lake 2. A) Drone image of Basque Lake 2 taken in February 2019. The segregated brine pools, more evident in (D), can still be seen under the snow cover. **B)** Ground photo of a sample site as we begin to drill the borehole array seen in the next panel. **C)** The typical sampling procedure where ice thickness and temperature are recorded, ice cores are gathered, and brine is extracted from the underlying lake. **D)** The lake without an ice cover, photographed in September 2019 (taken from hillside at top left of image A).

To prepare the samples for biological and chemical analysis, the ice samples were melted in a hot water bath within 18 hours of collection, and then both ice and brine samples were split for two workflows. One split involved aliquoting 45 ml of the unfiltered sample to a 50 ml Falcon tube and adding 2.5% glutaraldehyde to a final concentration of 0.25% to fix the cells for bioburden analysis. From that, 2 ml of the fixed solution was aliquoted into a cryotube for cell counting via flow cytometry (see below). All samples were then frozen at -20 °C and shipped frozen to either Scripps Institution of Oceanography (cryotubes) or Georgia Institute of Technology (Falcon tubes). Cell counts were acquired using two techniques: **1)** staining the cells with 4′,6-diamidino-2-phenylindole (DAPI) and imaging them using a Zeiss Epifluorescent Microscope (see Supplementary Section S1 for methods) and **2)** flow cytometry (Section 3.4) following the methods of [*Klempay et al.*, 2021]: in brief, fixed samples were stained with SYBR Green I nucleic acid dye (Molecular Probes) and spiked with a known quantity of 123count eBeads counting beads (Thermo Fisher). Samples were then run on a Guava easyCyte HT flow cytometer (Luminex). Flow cytometry outputs were analyzed in R using the flowCore library [*Ellis et al.*, 2009] and custom scripts.

For the second split we filtered the remaining sample (ice or brine) through a 0.2 μm polyethersulfone (PES) membrane Sterivex filter (filters were saved [frozen at -20 °C] for future work that will assess the community composition of these systems as part of the larger Oceans Across Space and Time project). The filtrate was then frozen at -20 °C and cold shipped to ALS Environmental in Tucson, Arizona for chemical analysis via ion chromatography (IC) and ion coupled plasma mass spectrometry (ICP-MS) methods. Samples were analyzed for the following ions: Br, Cl, F, NO_3, SO_4, CO_3 (alkalinity), Ca, Mg, K, and Na (Section 3.4) as well as total dissolved solids (TDS), pH, density, and conductivity.

3. Results

3.1 *Physical Properties of the Ice*

277 The ice cover of the lakes visited in both field campaigns was characterized by porous,
278 soft, cloudy/bubbly ice that was frequently damp with brine in all but the coldest ambient sampling
279 temperatures. The ice crystals had a lamellar structure similar to that of columnar sea ice (Figure
280 5a). The random orientation of the crystals is indicative of growth under quiescent conditions, as
281 expected for endorheic basins with limited flow. Upon drilling, the ice was noticeably odorous
282 (sulfur scented), an aspect that increased with depth, consistent with measurements indicating that
283 substantial amounts of volatiles were entrained within the ice cover (Supplementary Figure S3).
284 The basal portion of the ice cover (~5 cm) possessed visible brine channels (Figure 5b) similar to
285 those seen in sea ice.
286 These high porosity dendritic conduits are the byproduct of density driven convective
287 overturn in the lower layers of the ice [*Notz and Worster*, 2009]. In other systems where brine
288 channels are observed, this convective overturn proceeds as follows: As an ocean/brine freezes,
289 salts are rejected from the forming ice lattice, producing a porous ice matrix saturated with
290 hypersaline interstitial brine (a 'mushy layer' [*Feltham et al.*, 2006]). Where the porous ice matrix
291 is permeable enough to sustain Darcy flow (fluid flow in a porous media [*Bear*, 2013]) the cold,
292 saline, dense fluid at the top of the mushy layer downwells into the underlying fluid reservoir,
293 forming (dissolving) brine channels. The resultant porous basal layer of ocean/brine-derived ices
294 is capable of sustaining substantial thermochemical gradients that can provide metabolic energy
295 sources to any resident organisms [*Loose et al.*, 2011]. In sea ice this layer supports a substantial
296 biological community, including primary producers essential to the polar oceans (e.g., ice algae),
297 grazers, bacteria, and macrofauna [*Loose et al.*, 2011; *Tedesco and Vichi*, 2014]. Similarly, upon
298 ultraviolet irradiation, an ice core extracted from Salt Lake during the February 2019 season
299 exhibited visibly enhanced autofluorescence in the region adjacent to the ice-brine interface
300 (Figure 5c-d), suggesting an amplified presence of microbiota when compared to the upper portion
301 of the ice cover. This is corroborated by the quantitative biological profiles of Section 3.4.
302

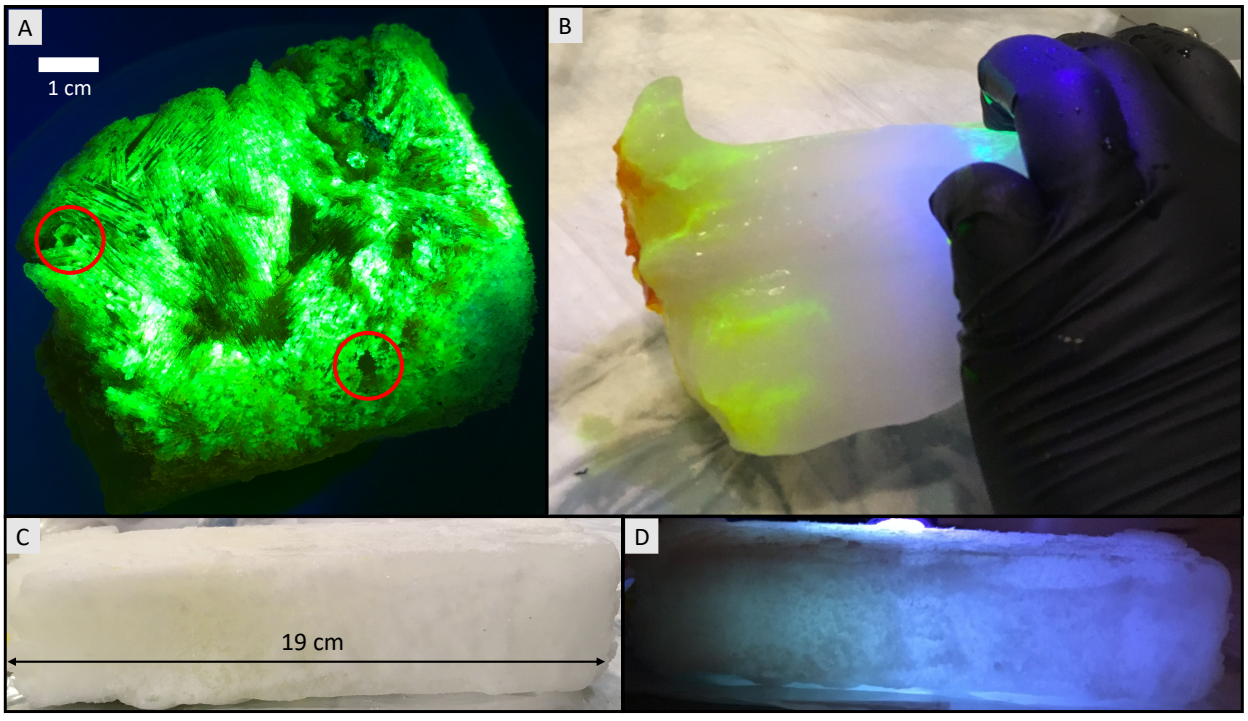

303

Figure 5 – Structural properties of Cariboo Plateau lake ices. A) Lamellar crystal structures at the base of an ice core from Salt Lake (February 2019). A fluorescein solution was poured onto the base of the inverted ice core and it was illuminated with an ultraviolet (UV) flashlight. The openings of two brine channels can are circled in red. **B)** Brine channels in the basal layer of the Salt Like ice core pictured in frame A. We melted the edges of the ice core away by running it under water, revealing locations where fluorescein had percolated into the ice core via brine channels (again, illuminated by a UV flashlight). **C)** Salt Lake ice core before fluorescein was added (visible light). Bottom of the core is to the left of the image. **D)** Same as panel D under UV illumination. Autofluorescence is evident near the base of the ice core, indicating the presence of microorganisms.

3.2 *Stratigraphy of the Ice-Brine Lake Systems*

During the winter most of the lakes possess four primary layers; (1) an ice cover, (2) a shallow (<1 m thick) brine layer, (3) solid salt hydrates (See Supplementary Figure S2), and (4) underlying sediments. Stratigraphic profiles of 12 sample sites visited during February 2020 can be seen in Figure 6. Most sites have the expected ice→brine→salt hydrate→sediment vertical layering that occurs when salts are rejected from the forming ice cover, saturate the underlying brine, and precipitate out of solution, forming a salt hydrate layer atop the underlying sediments. However, there are a number of interesting exceptions as well as additional layering features that may provide further insight into the physical and geochemical evolution of these systems. Typically, deeper lakes are fresher and thus may not reach their saturation points during winter (e.g., Salt Lake – note the limited freezing point depression of the sub-ice brine [Figure 7]). An exception is Basque Lake 1 sample Site 3, which possessed a salt hydrate layer suggesting the lake brine is saturated; this is reasonable given the extremely low temperature of the brine [Figure 7]. Other interesting features include: **i)** an intra-ice brine layer observed in the ice cover of Basque Lake 2 sample Site 2 that may be indicative of eutectic melting in the ice or over pressurization of the underlying brine (if progressive freezing is not compensated by ice uplift); **ii)** the alternating layers of salt and sediment at Basque Lake 4 sample Site 2 indicating localized salt precipitation features (note the lack of a salt layer for Basque Lake 4 sample Site 1) that are likely the remnant 'crystal bowls' [*Renaut and Long*, 1989] of previously existing brine pools (see Figure 2 of [*Foster et al.*, 2010]); **iii)** the confirmed existence of a substantial salt basement beneath the lakes (e.g. Basque Lake 4 sample Site 2 – in many cases there likely exists a salt hydrate basement beneath the lowest sediment layer measured [*Jenkins*, 1918; *Renaut and Long*, 1989]); **iv)** two visibly distinct salt hydrate layers at the base of Last Chance Lake (a 1 cm layer overlying a 5 cm layer – Supplementary Figure S2). The geophysical and biogeochemical implications for both terrestrial and planetary environments are discussed in Section 4.

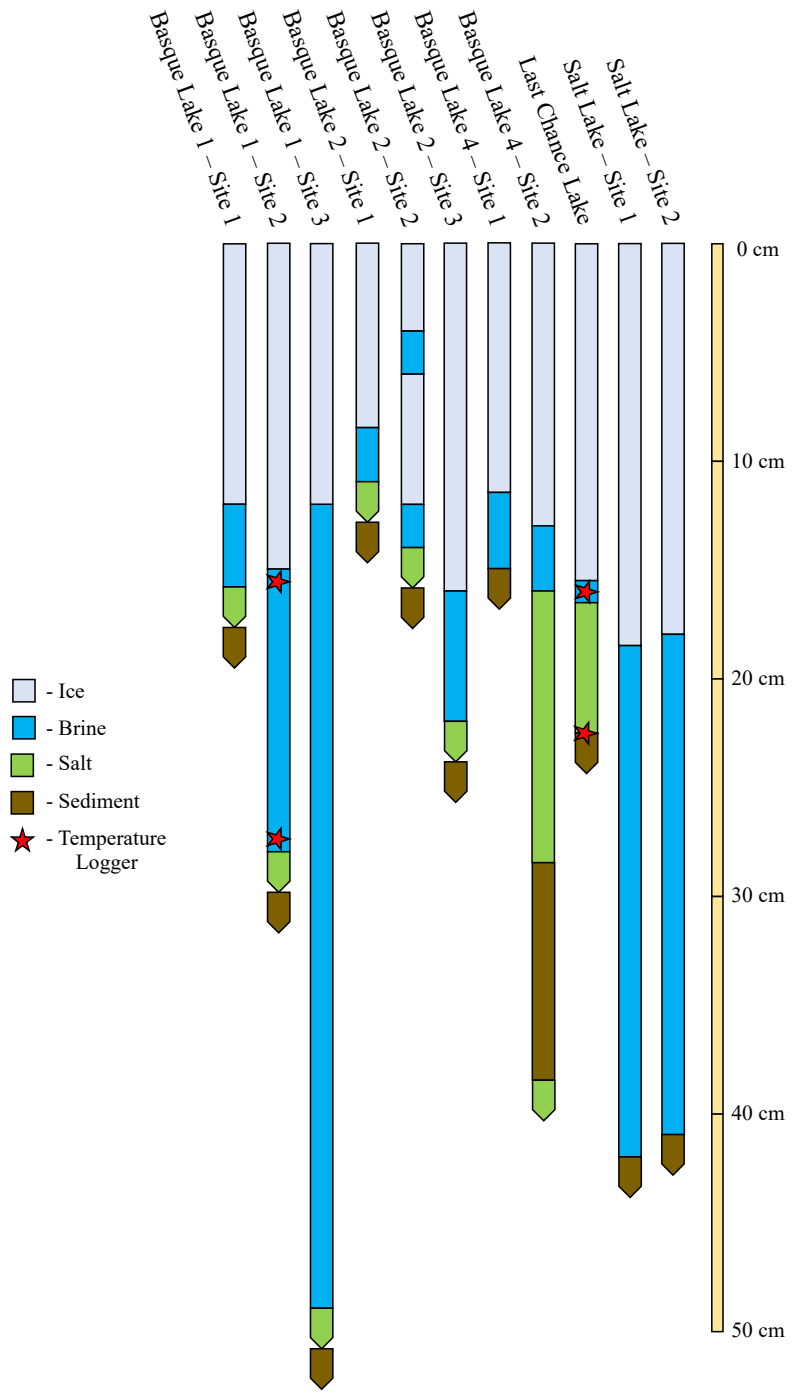

Figure 6 – Stratigraphic profiles of select February 2020 sample sites. Portions of the profiles represented by bars with squared ends have known thicknesses. Portions of the profile with pointed ends have unknown thicknesses (either they were too thin to measure, too thick to extract, or were the lowest layer accessed).

3.3 *Temperature Profiles*

We acquired two distinct temperature datasets during our 2019 and 2020 February field campaigns. The first consists of vertical temperature profiles for all extracted ice cores. The second

consists of hourly air and brine temperature records from September 2019 to February 2020, obtained using HOBO temperature sensors.

3.3.1 *Ice Core Temperatures*

Ice and brine temperature profiles for all sites visited in 2019 and 2020 can be seen in Figure 7. Due to consistently colder ambient air temperatures (Figure 7; 0 cm), the temperature profiles for the 2019 ice covers are much more monotonic, where temperatures increase with depth – profiles lacking brine measurements entirely indicate ponds which were frozen to the sediment bed. Conversely, high daytime temperatures during February 2020 can be seen warming the near surface ice, in many cases to values that exceed the temperatures deeper in the ice column. Profiles without brine measurements are frozen to the sediment bed. Brine temperatures ranged from -5.31°C to -0.53°C and are significantly below the freezing point of fresh water due to the presence of dissolved salts (Section 3.4). An inter-ice brine layer (~0.5-2 cm thick) was observed at Basque Lake 2 sample Site 2 in February of 2020 (Figure 7; filled red square at ~5 cm). This unique feature has important implications for the potential generation of brines in the icy regolith of Mars and ice shells of ice-ocean worlds. We discuss potential formation mechanisms for the layer as well as its astrobiological relevance in Section 4. It is not uncommon for salt hydrate layers to occur at the base of the lakes (Section 3.2), however extraction of these layers through holes in the ice cover is far from straightforward. With strengths and hardnesses that exceed those of ice [*Durham et al.*, 2005] even thin layers (~6 cm) must be chiseled through. In 2020 at Last Chance Lake sample Site 1, the wooden stake holding the HOBO temperature sensors was firmly encased by the salt hydrate layer at the base of the lake, with one temperature sensor attached to the stake below the hydrate layer (See Figure 4 and Section 3.3.2). To extract the temperature sensor, the hydrate layer was chiseled through with a hammer and metal rod (Supplementary Figure S2). Exceptionally warm temperatures (-0.3°C and -0.5°C) were measured in both of the distinct hydrate layers described in Section 3.2 (green circles of Figure 7). The potential importance of salt hydrates in these and analogous planetary ice-brine systems is discussed in Section 4.

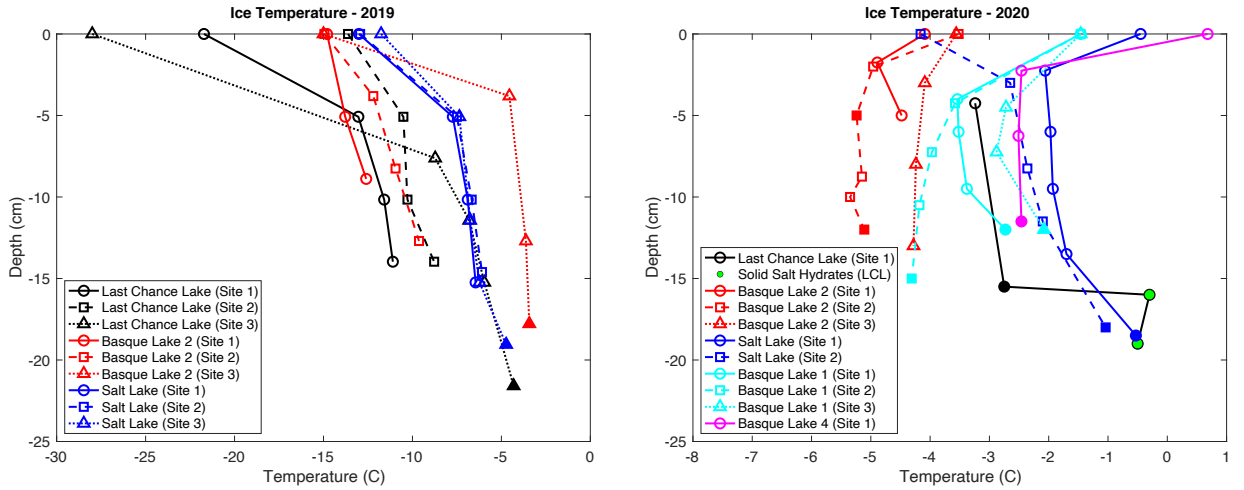

Figure 7 – Ice cover temperature profiles. Left) Vertical ice core temperature profiles taken during February 2019. Filled symbols signify a brine temperature. **Right)** Vertical ice core temperature profiles taken during February 2020. At Last Chance Lake two distinct salt hydrate layers had precipitated just above the lake sediments. Note the unique interior brine layer at the Basque Lake 2 Site 2 location. (Note: probe thermometer accuracy is 0.01 °C)

3.3.2 *Seasonal Temperatures*

During September 2019 six HOBO temperature loggers were installed at the hypersaline lakes (three at Last Chance Lake, three at Basque Lake 2). At each lake one temperature logger was attached to a nearby tree to measure air temperature. The other two loggers were affixed to a wooden stake with zip ties and driven into the sediments of a brine pool. One logger was placed near the brine-sediment interface, the other was placed in the middle of the water column. Between September 2019 and February 2020, the loggers recorded hourly temperature readings, the results of which can be seen in Figure 8. At the time of extraction both temperature loggers were in the sub-ice brine layer of Basque lake 2. At Last Chance Lake one temperature logger was in the sub-ice brine layer, the other was beneath a 6 cm layer of precipitated salt hydrates (See Figure 6 for exact locations). During the fall large diurnal variations in temperature occur in both the air and brine. Upon the formation of an ice cover in late November the brine becomes extremely well insulated and no longer varies appreciably on a diurnal scale. The minimum brine temperatures recorded were -6.37°C (December 1) and -8.45°C (November 30) for Basque Lake 2 and Last Chance Lake, respectively. The subsequent warming of the brines and a lack of any appreciable temperature variations after the brines reached their minimum temperatures (even under substantial cooling that occurred mid-January), suggests significant insulation by the overlying ice, a substantial heat source due to salt hydrate precipitation in the underlying brine, or both. An early season minimum brine temperature followed by a significant temperature increase (red boxes, Figure 8) favors the presence of the latter, as it appears the brine becomes supercooled, precipitates salt hydrates, and then remains at or near its eutectic temperature (no longer requiring supercooling/supersaturation to nucleate salt hydrates as a substrate already exists for continued precipitation [*Toner et al.*, 2014]). Further discussion of this process and its relevance to both terrestrial and planetary ice-brine systems is included in Section 4.

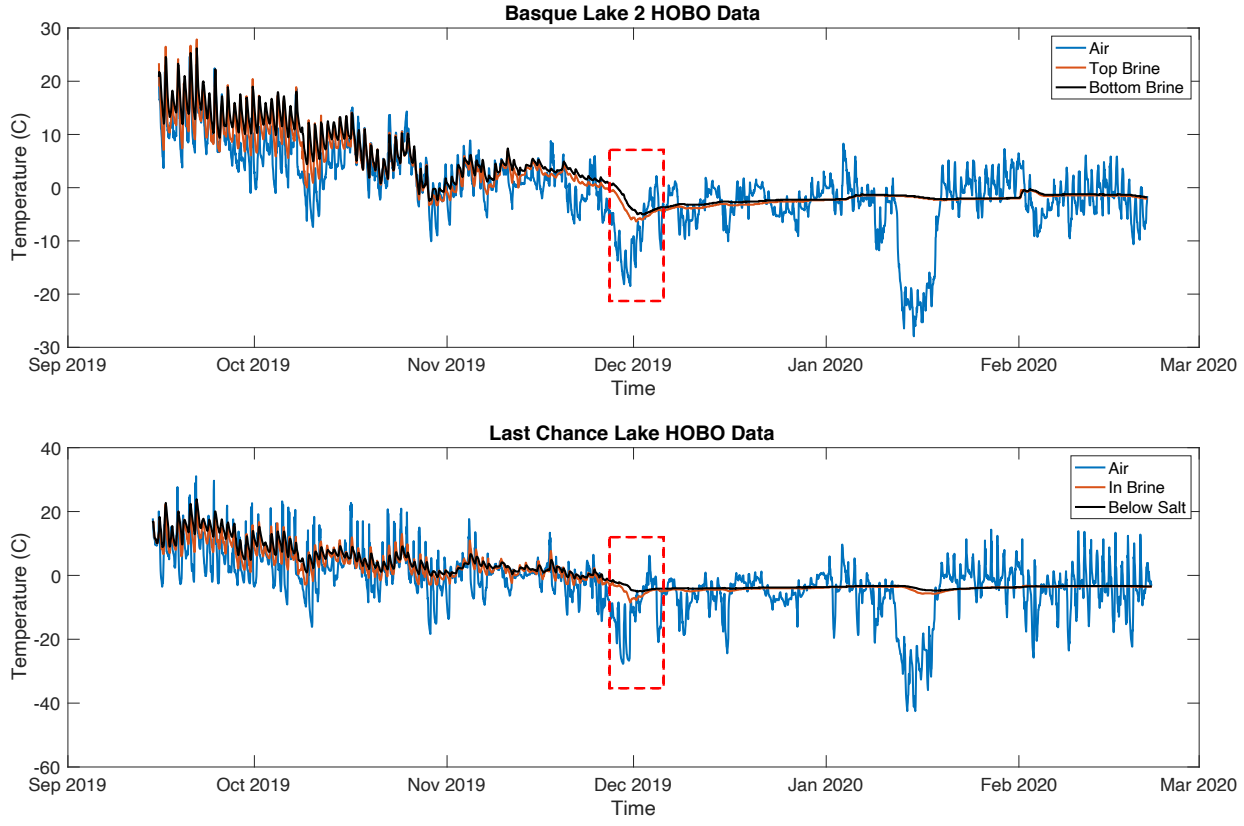

Figure 8 – Seasonal variations in air and brine temperatures. Top) Hourly temperature data for Basque Lake 2. **Bottom)** Hourly temperature data for Last Chance Lake. (Red boxes highlight early season brine temperature minimums and subsequent brine warming, potentially indicative of brine supercooling and latent heat release due to salt hydrate precipitation, respectively.)

3.4 *Major Ion & Bioburden Profiles*

Bioburden and chemical profiles from each lake were derived using ion chromatography (IC), ion coupled plasma mass spectrometry (ICP-MS), fluorescence microscopy, and flow cytometry (FCM). The vertical distribution of major ions in each lake (ice cover and underlying brine) are shown in Figure 9. All three of the Basque Lakes sampled (1, 2 and 4) as well as Salt Lake were dominated by sulfate with the second most abundant ion being magnesium. Last Chance Lake was dominated by carbonate, sodium, chloride, and sulfate with a negligible concentration of magnesium. Basque Lake 2 had the highest ionic concentration of all the lakes. A number of the ion profiles have 'c-shaped' distributions, with high ion content in the near surface ice, lower ion content in the middle portion of the ice column, and increasing ion content approaching the base of the ice column and underlying brine, similar to the characteristic bulk salinity profile of first year sea ice [*Eicken*, 1992; *Malmgren*, 1927]. The amplifications near the surface are due to rapid freezing as heat is lost to the colder atmosphere before salt can be rejected into the underlying fluid. Amplifications near the base of the ice are due to the ice-brine interface existing as a porous two-phase layer, composed of a solid ice matrix bathed in concentrated interstitial brine – a ubiquitous feature of ice formed from saline solutions (e.g., [*Buffo*, 2019; *Feltham et al.*, 2006]). A number of exceptions to the 'c-shaped' trend exist in our observations: **i)** exceptionally low ion contents in the shallow ice of Salt Lake (Figure 9a) which we have reason to believe is due to analysis error, as the reported ion concentrations are not charge balanced, **ii)** only one ice sample from Last Chance Lake was acquired due to exceptionally warm temperatures (deeper ice had excessive brine infill and could not be adequately cored without contamination from the infilling brine), **iii)** an internal brine layer existed in the ice cover of Basque Lake 2 (see Figure 6), which exhibited exceptionally high ion concentrations (and cell densities).

Vertical microbial cell density distributions for all of the lakes are shown in Figure 9. Cell densities tend to increase with depth – with the notable exception of Basque Lake 2 – which features an inter-ice brine layer. This inter-ice layer was located 5 cm below the surface and contained almost twice the cell concentration (2.503×10^6 cell ml^{-1}) as the three other depths measured in the ice cover (1.449×10^6, 1.229×10^6, and 1.358×10^6 cell ml^{-1}). Salt Lake had a noticeable peak of cell density at a depth of 13.5cm which then decreased slightly in the subsequent brine layer. Last Chance Lake had the lowest basal brine cell density. The geophysical and astrobiological implications of the observed cell densities and major ion distributions are discussed in Section 4.

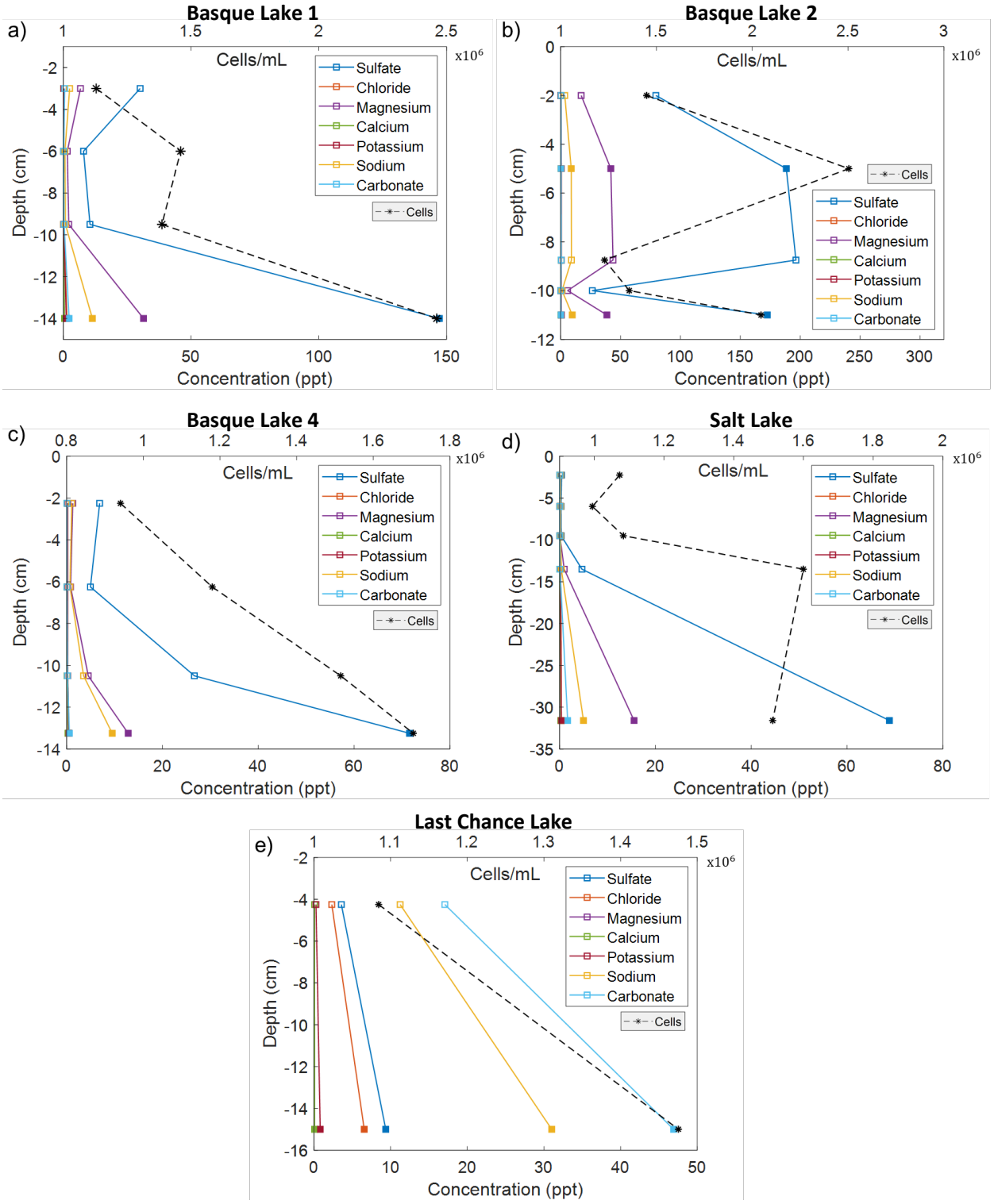

Figure 9 – Major ion and cell density profiles of selected lake sites. a) Basque Lake 1 – exhibiting a 'c-shaped' ionic profile and a general increase in cell density as the ice-brine interface is approached. **b)** Basque Lake 2 – with amplified salt and cell concentrations in the internal brine layer ~5 cm below the surface, even exceeding those of the underlying brine. Basque Lake 2 is the most concentrated lake of the Basque Lakes sampled and contains a higher cell density in the top ice layer than the other lakes. **c)** Basque Lake 4 – similar to Basque Lake 1, Basque Lake 4 exhibits

a 'c-shaped' ionic profile and a trend of increasing cell density with depth. Basque Lake 4 has a lower $MgSO_4$ concentration and lower cell density in its underlying brine than the other Basque Lakes. **d)** Salt Lake – there exists a spike in cell density in the bottom ice sample, around -13.5cm, exceeding that of the brine sample at -32cm. **e)** Last Chance Lake – only one ice sample was obtained during February 2020 due to warm temperatures. Last Chance Lake is the only Na-CO_3 rich lake sampled and has the lowest cell density in its underlying brine. All ionic concentration and cell density values can be found in Supplementary Table S1 and Table S2, respectively. (Note: filled symbols represent brine samples).

3.5 *Permeability*

One of the primary controls of fluid and solute transport in ocean and brine derived ices (e.g., sea ice) is the permeability of the ice cover. Desalination of the ice, through both gravity drainage and surface flushing, depends critically on the flow of brine and meltwater through the ice, and in turn governs the resultant salinity distribution in the ice [*Notz and Worster*, 2009]. In high porosity (generally highly permeable) regions near the ice-ocean interface, nutrient and detritus transport is a crucial process governing the productivity and sustainability of biological communities that thrive in the interstitial brine [*Loose et al.*, 2011; *Thomas and Dieckmann*, 2003]. It stands to reason that fluid transport, and thus permeability, likely plays an equally important role in the biogeochemical evolution of the hypersaline ice-brine systems investigated here.

In February 2020, it was relatively warm (air temperatures exceeded 0 °C by mid-morning) the day Last Chance Lake was sampled. Ice cores were extracted at one site, however by the time a second site was selected, rapid brine infill into boreholes of all depths precluded coring as inflowing brine from the underlying reservoir would contaminate ion and bioburden estimates. Taking advantage of the highly porous ice we conducted three slug test experiments (borehole depths of 6cm, 8cm, and 10cm) to investigate the permeability of the ice cover, the results of which can be seen in Figure 10. These recovery curves track the hydraulic head of the brine infilling the borehole over time. Here hydraulic head is equivalent to the difference between the height of the infilling brine and the freeboard level. This is a common technique used in sea ice research, and it can be shown that the temporal evolution of the hydraulic head is related to permeability via *Freitag and Eicken* [2003]:

$$h(t) = h(t_0) \exp\left(-k \frac{g\rho t}{\eta L}\right) \qquad (1)$$

where $h(t)$ is the hydraulic head at time t, $h(t_0)$ is the hydraulic head at the onset of the slug test, k is permeability, g is gravity, ρ is brine density, η is the dynamic viscosity of the brine, and L is the distance between the bottom of the borehole and the base of the ice cover. Best fit curves of this functional form have been applied to all three slug test experiments and can be seen plotted against the data in Figure 10. Our measurements are well represented by the decaying exponential of Equation 1. As borehole depth increases the quality of the fits decreases. This is likely due to increased lateral brine infiltration in deeper boreholes. Equation 1 assumes only vertical brine infiltration from the base of the borehole. While this is likely the main source of brine infiltration, the sides of the borehole will also experience a nonzero amount of lateral infiltration. Deeper boreholes have larger sidewall surface areas and thus will be more affected by this process. Typically, studies implementing the slug test technique will deploy a hollow cylindrical casing to minimize the effects of lateral brine infiltration. The impromptu nature of our study left us wanting in this regard and would have likely reduced the amount of misfit in our deeper borehole measurements. Nevertheless, we can use the exponential coefficients of our fit lines and Equation 1 to acquire upper bound estimates of the ice permeability. The permeabilities of the 6cm, 8cm,

and 10cm boreholes are 1.6e-10 m^2, 1.2e-10 m^2, and 6.3e-11 m^2, respectively. There is a slightly decreasing trend in permeability with depth, which could correlate to enhanced porosities in the rapidly cooled, near surface ice (e.g. [*Buffo et al.*, 2018]). As the ice-brine interface is approached permeabilities increase dramatically, evidenced by boreholes drilled below 10cm infilling with brine too rapidly to accurately measure the change in hydraulic head. The estimated permeabilities of the Last Chance Lake ice fall in the center of permeabilities observed in natural and laboratory grown sea ice, which range from 10e-13 m^2 to 10e-7 m^2 (see Figure 7a of *Freitag and Eicken* [2003]).

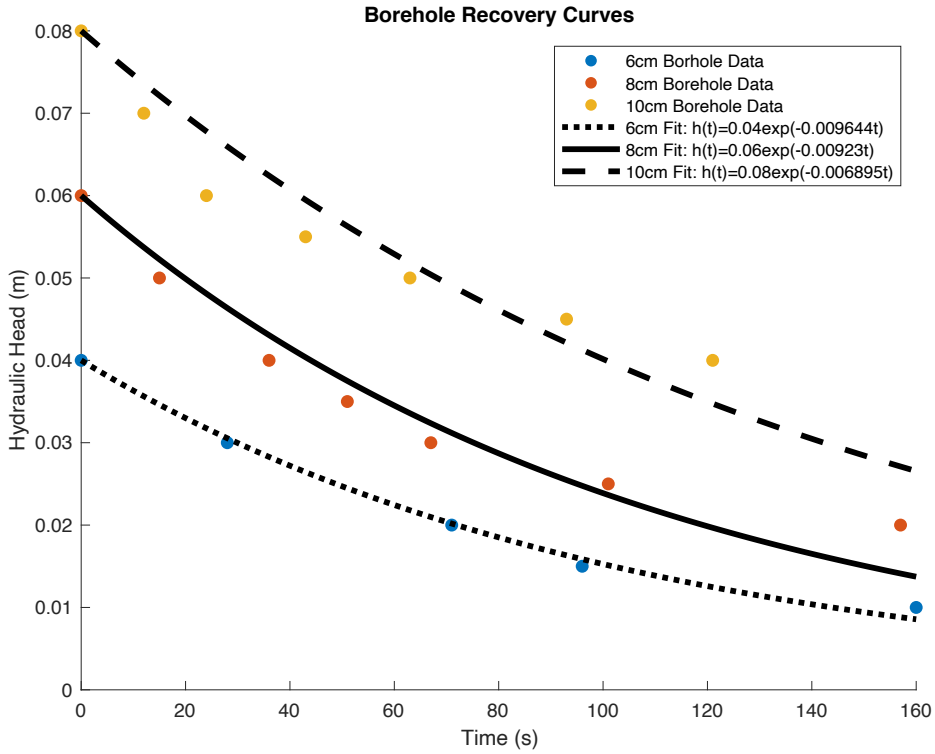

Figure 10: Slug test recovery curves used to estimate ice permeability. Temporal variations in hydraulic head are measured as brine infills three boreholes of different depth (6cm, 8cm, and 10cm from the ice surface). Exponential decay curves (Equation 1) are fit to the hydraulic head measurements (based on the method presented in [*Freitag and Eicken*, 2003]).

3.6 *Porosity*

Permeability is largely driven by porosity (ϕ), which plays an important role for both thermophysical and biogeochemical processes in ice-brine systems. Porosity, or liquid fraction, aids in facilitating solute (e.g. salts, nutrients, waste) transport throughout the ice via connected brine networks. Similar to sea ice, higher porosity regions will likely be associated with amplified fluid flow, while low porosity regions should limit fluid flow and trap brines in discrete brine pockets as flow networks become more disconnected upon continued solidification [*Golden et al.*, 1998; *Golden et al.*, 2007]. The complex microstructure of saline ices, coupled with their physical and thermal fragility, makes direct measurements of ice porosity quite challenging in the field. Even in laboratory settings the utilization of micro computed tomography (micro-CT) methods to measure ice porosity must carefully control the temperature of the sample to avoid melting, freezing, and redistribution of the fluid phase (e.g. [*Golden et al.*, 1998; *Golden et al.*, 2007; *Maus*

et al., 2020]). Fortunately, there exists a link between the temperature, ionic composition, and liquid fraction of a solution. Conceptually similar to the eutectic phase diagrams of simpler binary or ternary solutions, equilibrium and fractionation chemistry models (e.g. FREZCHEM [*Marion et al.*, 1999], PHREEQC [*Parkhurst and Appelo*, 1999; 2013], SeaFreeze [*Journaux et al.*, 2020]) are able to utilize Pitzer equations or Gibbs free energy approaches to predict the composition and phase evolution of a solution as it is frozen.

Here, we use PHREEQC, our *in situ* ice temperature measurements (Section 3.3.1), and our ionic concentration measurements (Section 3.4) to estimate the porosity (liquid fraction) of the ice covers (Figure 11). The colder atmospheric temperatures present during February 2019 result in low porosities (0.008-0.086) and porosity profiles which generally increase with depth. Conversely, the warm surface temperatures during the February 2020 campaign result in higher overall porosities (0.019-0.227), particularly in the warm shallow ice layers, likely due to melting/dissolution of the ice. This link between warm surface temperature and high porosities may provide an explanation for the brine layer observed at Basque Lake 2. If the shallow ice was warmed to a point where solutes could be mobilized in the pore space of the ice (e.g., by air temperatures >0 °C [Figure 8]), they would percolate downward until they reached an impermeable layer (e.g., colder ice [Figure 7]), potentially producing a highly saline region within the ice. This high salinity region could lead to the dissolution of the surrounding ice, ultimately producing the observed internal brine layer. It is interesting that many of the estimated porosities are near the sea ice percolation threshold (ϕ_c) of ~0.05, predicted by *Golden et al.* [2007]. This suggests that solutes are mobile in the ice cover when $\phi > \phi_c$, and when freezing occurs salination of the interstitial fluid leads to gravity drainage [*Notz and Worster*, 2009] and freshening of the pore fluid. This allows for continued freezing of the ice layer. However, once the porosity is ~0.05 ($\phi \approx \phi_c$) the percolation limit is reached and fluid flow within the ice is drastically reduced, preventing freshening of the pore fluid via gravity drainage and inducing a slower continued freezing rate of the residual brine as it is further concentrated (i.e., its freezing point is further reduced), resulting in the clustering of porosities around 0.05. Porosities ~0.05 are in the range observed for seawater-derived ices at similar temperatures (e.g. [*Golden et al.*, 2007]). This is expected even for the amplified ion concentrations in the magnesium sulfate dominated ices as $MgSO_4$ has less of an impact on freezing point depression than does NaCl. This chemistry-dependent variability in freezing point depression is also evidenced by the amplified porosities (and lower minimum brine temperatures) seen at Last Chance Lake, which has a higher concentration of sodium chloride. The implications of porosity for material transport, astrobiology, and the geophysics of planetary ices is discussed in Section 4.

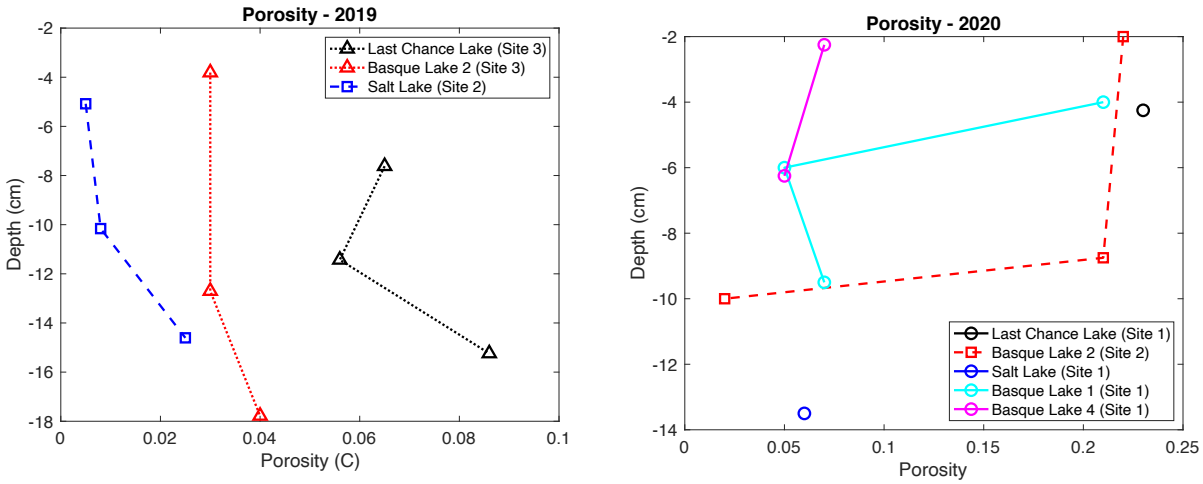

Figure 11: Porosity profiles within the lake ice covers. Left) Porosity of the lake ice covers during February 2019. **Right)** Porosity of the lake ice covers during February 2020. Symbols and colors correspond to those presented in the temperature profile plots of Figure 7.

4. Discussion

The compositionally diverse hypersaline lakes of south-central British Columbia offer a unique analog laboratory to constrain the physicochemical properties and dynamics of planetary relevant ice-brine systems. The identification of relationships between the bioburden and ionic composition of chemically diverse ices, their formation histories, and their underlying parent fluid properties as well as the observation of thermophysical features theorized to occur in planetary ice-brine environments (e.g., inter-ice hydrologic features, supercooling, salt hydrate precipitation) has both geophysical and astrobiological implication for icy worlds in our solar system.

4.1 *Physicochemical and Biological Stratigraphy of the Ice-Brine Systems*

The general trends in major ion content, cell density (bioburden), porosity, and permeability suggest a dynamic ice cover capable of fluid, solute, and biological transport. As the ice solidifies, rejects salts into interstitial brine veins and pockets, and the brine concentrates, the system becomes gravitationally unstable and the interstitial brine convects downward into the underlying brine reservoir, forming brine channels in the ice (Figure 5) [*Buffo et al.*, 2021a]. The freshened ice can thus continue freezing, leading to a trend of increasing porosity and permeability with depth in the ice cover. While the upper layers of the ice cover typically possess lower bulk ion concentrations than the underlying fluid, the remaining salts are likely concentrated in residual brine pockets, making any liquid regions in the upper ice column highly saline and potentially less hospitable to any resident organisms. The lower liquid content, generally colder temperature, and potentially chaotropic brine in the upper layers of the ice suggest that lower portions of the ice cover are likely to provide greener pastures for any biology present in the system (a trend mirrored in fresh lake ice [*Santibáñez et al.*, 2019] and sea ice [*Loose et al.*, 2011; *Tedesco and Vichi*, 2014; *Thomas and Dieckmann*, 2003]). Indeed, the bioburden profiles of all the lake ice covers show amplified cell densities in the basal ice and underlying brine. In the case of Salt Lake, the highest cell density in the ice-brine system was observed within the basal ice layer. This is consistent with observations of sea ice, where volumetric ice algae densities in the lower layer of the ice column typically far exceed those of the underlying ocean [*Ackley and Sullivan*, 1994; *Spindler*, 1994]. This feature may have been most prominent at Salt Lake due to the deeper (> 20 cm) underlying

water column, as the benefits of colonizing the porous basal ice layer may not have been as prevalent in the shallower lakes due to the proximity of the brine-sediment interface – another advantageous substrate for biology to thrive within. It is important to note that there was appreciable biology present in all samples, including the shallow ice regions. While exploration of the viability of cells located in different regions of the ice cover was beyond the scope of this study, our results suggest that substantial bioburden (viable or not) is entrained in diverse saline ices and that the density of the entrained bioburden is related to the ice formation history and underlying brine properties (e.g., brine chemistry, brine bioburden, ice liquid fraction). A similar quantitative relationship between salt entrainment and ice formation history has been shown to be important in describing the geochemistry of planetary ice shells [*Buffo et al.*, *2020; Chivers et al.*, 2021; *Hammond et al.*, 2018; *Vance et al.*, 2020]. Constraining the rates of impurity entrainment in saline ices has important implications for our understanding of ice-ocean worlds, where ice shell geophysics depend critically on material properties of the ice [*Durham et al.*, 2005; *Han and Showman*, 2005; *McCarthy et al.*, 2011; *Pappalardo and Barr*, 2004], biosignature expression is dependent on the entrainment and transport dynamics of the ice shell [*Schmidt*, 2020; *Schmidt et al.*, 2017] and constraining the habitability of the underlying ocean will lean heavily on the interpretation of spacecraft measurements of the ice shell [*Howell and Pappalardo*, 2020].

4.2 *The Internal Brine Layer*

The internal brine layer observed at Basque Lake 2 sample Site 2 is of substantial interest as it supports the idea that high porosity water rich regions may persist in the upper layers of an ice column. While similar environments have been repeatedly observed in meteoric ice (e.g., firn aquifers, brine infiltration into the McMurdo Ice Shelf) the occurrence of discrete internal brine layers in ocean/brine derived ices is much more limited. Brine layers have been observed in cryopegs [*Gilichinsky et al.*, 2005; *Gilichinsky et al.*, 2003; *Iwahana et al.*, 2021; *Shimanov et al.*, 2020], marine permafrost [*Colangelo-Lillis et al.*, 2016], and a limited number of Antarctic Dry Valley lake ice covers [*Priscu et al.*, 1998]. In the case of Basque Lake 2 a solid ice layer overlayed a discrete brine pocket which we were able to drain by syringing brine out (<1 L total volume). The brine layer thickness varied locally from 0.5-2 cm in thickness. The brine layer was not present at drill sites < 1 m away, thus the brine layer was highly localized and not substantially connected to the basal brine layer (as there was no inflow into the voided pocket). We do not know the exact physical processes which would facilitate the generation of such an internal brine layer but propose that eutectic melting of a high salinity region due to surface warming or pressurization of the underlying brine pool as potential mechanisms. If there existed a region of enhanced salinity within the ice cover warming from the surface could raise the internal ice temperature above its eutectic melting point, creating a localized melt pocket/sheet which would grow in volume through dissolution of ice until the concentration of the melt pocket was such that its freezing point matched the local temperature. Such high salinity regions could form due to localized interstitial hydrate precipitation during a period of rapid ice formation, or from the collection of downwelling melt created by warm surface temperatures when it reached an impermeable layer. The low temperature of the internal brine (-5.24°C), its similarity to the basal brine temperature (-5.11°C, which is likely at its saturation point), and their separation by a colder ice layer (-5.35°C) would support the latter theory. Conversely, over pressurization of the underlying brine pool could drive upward brine transport into porous regions of the ice cover. The relatively small size of the brine pools, along with the low permeability of the surrounding sediments and underlying salt hydrate basements (Figure 1), could facilitate over pressurization in the basal brine and force brine upwards into the

ice cover, where it would preferentially infiltrate porous regions/layers of the ice (akin to sill intrusion in magmatic systems). If the conduit sourcing the brine layer refroze it could isolate the intra-ice brine, forming the observed feature.

While occurring on a smaller scale in the lake ice cover, these exact processes have been theorized as mechanisms that could induce analogous cryovolcanic/cryohydrologic processes in the ice shells of ice-ocean world (e.g. lens formation via eutectic melting [*Schmidt et al.*, 2011], sill and dike formation via intrusion of underlying ocean fluid [*Craft et al.*, 2016; *Michaut and Manga*, 2014]). Such near surface liquid environments would provide accessible targets for upcoming missions, important for both planetary exploration and planetary protection. As such, understanding the generation, distribution, longevity, and potential habitability of such features is imperative to constraining the spatiotemporal habitability of such worlds and will inform mission design and data synthesis. Similarly, salt rich aqueous environments on both ancient (e.g. [*Fastook and Head*, 2015; *Fastook et al.*, 2012; *Ojha et al.*, *2020*]) and present day (e.g. [*Lauro et al.*, 2020; *Ojha et al.*, 2015; *Orosei et al.*, 2018]) Mars would likely be characterized by cryohydric processes, some exceptionally similar to the Canadian lakes we visited [*Fox-Powell and Cockell*, 2018; *Fox-Powell et al.*, 2016; *Pontefract et al.*, 2019; *Pontefract et al.*, 2017]. These unique analog systems can be leveraged to improve habitability classifications for Martian regions, quantify putative Martian hydrological processes, and aid in the search for remnant, relict, and contemporary habitable environments.

4.3 *Supercooling and Salt Hydrate Formation*

Another interesting process observed at the lakes is supercooling, the depression of a liquid below its freezing point. Evidence for supercooling can be seen in the seasonal evolution of brine temperatures at Basque Lake 2 and Last Chance Lake (Figure 8). The minimum brine temperatures occur early in the season, likely before any basal salt hydrate layer is present (e.g., in September 2019 there were no basal hydrates present at Last Chance Lake – compare to Supplementary Figure S2). The lack of nucleation sites for precipitation to occur requires the brine to supersaturate and supercool until the energy barrier for initial salt hydrate nucleation is overcome [*Toner et al.*, 2014]. Once this minimum temperature is reached and an initial basal salt layer is established, further precipitation occurs at the eutectic temperature and concentration of the sub-ice brine (no supercooling is needed to facilitate further nucleation as there now exists nucleation sites). This leads to stable brine temperatures, evident in both lakes for the remainder of the season (Figure 8). Only minimal deflections in brine temperature occur, even under extreme surface temperature variability (e.g., multiple days of surface temperatures $\leq$-15°C during mid-January and multiple days of surface temperatures above the brine eutectic temperatures in early February). A principal explanation for the exceptional stability of the sub-ice brine temperatures is the large latent heat of fusion associated with precipitation of both ice and salt hydrates, which can have latent heats of formation that exceed that of the ice-water phase transition by orders of magnitude [*Grevel et al.*, 2012]. A substantial heat source and sink, the energy associated with the phase change of these materials will buffer any drastic and rapid changes in brine temperature. Additionally, the precipitation of salt hydrates upon saturation of the sub-ice brine substantially increases the longevity of the fluid reservoir, as all of the heat associated with the latent heat of formation of the hydrates must also be lost from the system before solidification of the brine can continue. This is supported by ice thickness measurements of Little Salt Pond, a substantially less saline spring-fed pool adjacent to Salt Lake (~100 m), which exhibited an ice thickness of 31 cm compared to Salt Lake's measured ice thicknesses of 18 cm and 18.5 cm.

Supercooling and salt hydrate precipitation have important implications for low temperature saline systems on Earth, Mars, and ice-ocean worlds. The observation of supercooling in naturally occurring brines on Earth gives credence to the possibility for analogous supercooled environments on other bodies (e.g. [*Toner et al.*, 2014]) and is a unique extremophilic habitat in its own right. If these supercooled environments can persist for geologically significant time scales, they could broaden the thermal limits where liquid water is stable, and thus the window of the limits of life. We note that the time scale over which the brines observed in this study remain supercooled is on the order of days, however the Canadian lake systems are minimally buffered from the local extreme surface temperatures. If a brine system on Mars or Europa was buried in the subsurface regolith or ice shell it would likely be subject to more gradual thermal variations and could potentially remain in a supercooled state for much longer. The antifreeze potential associated with salt hydrate precipitation could be even more impactful. In magnesium sulfate systems, one of the first stable hydrate phases is meridianiite ($MgSO_4 \cdot 11H_2O$). With a latent heat of formation of $1.44e^7$ J/kg [*Grevel et al.*, 2012] (~43 times that of ice) its precipitation releases an immense amount of heat into saturated magnesium sulfate systems (i.e. the lakes observed in this study). This suggests that if ice-brine systems reach saturation and begin to precipitate out salt hydrate phases, their continued solidification could be drastically impeded, significantly extending their lifetimes. These salt rich niches could provide stable (or quasi-stable) aqueous environments for halophilic psychrophiles, water activity and chaotropicity permitting. Potential regions where this phenomenon could (have) occur(ed) include surface and shallow subsurface saline lakes and sediments on Mars [*Rapin et al.*, 2019; *Toner et al.*, 2014], subglacial Martian lakes [*Lauro et al.*, 2020; *Orosei et al.*, 2018; *Sori and Bramson*, 2019] similar to some terrestrial hypersaline subglacial systems [*Rutishauser et al.*, 2018], and hydrological brine features in the ice shells of ice-ocean worlds (e.g. lenses and lenticulae [*Chivers et al.*, 2021; *Schmidt et al.*, 2011], sills, dikes, porous regions [*Buffo et al.*, *2020*]). Constraining the physical, biological, and chemical dynamics of these understudied analog environments will feed directly into forward models of planetary ice-brine environments aimed at quantifying their spatiotemporal evolution, habitability, and dynamic processes.

The presence of salt hydrates in ice-brine systems can add additional geochemical complexities. When salt hydrates precipitate out of solution, they introduce new phases to the system and alter the chemistry of the remaining brine. Much like fractional crystallization in magmatic systems, this can result in chemical heterogeneity of the resulting solid and will govern the chemical evolution of the residual melt [*Fox-Powell and Cousins*, 2021]. In analogy with terrestrial petrology of the mantle and lithosphere, minimal variations in melt fraction and composition can have substantial impacts on the thermal and mechanical properties of planetary ice shells [*Buffo et al.*, 2021b; *McKenzie*, 1989]. Furthermore, models aimed at interpreting the relationship between ice composition and parent fluid composition and/or habitability (e.g. linking surface ice or plume particle composition to interior ocean composition) should address the potential effects of salt hydrate precipitation dynamics as fractional crystallization could alter the results [*Buffo et al.*, *2020; Fox-Powell et al.*, 2020; *Fox-Powell and Cousins*, 2021]. Currently, dynamic models of planetary ices and ice-ocean world systems do not account for the presence or effects of salt hydrates [*Buffo et al.*, *2020; Buffo et al.*, 2021b; *Vance et al.*, 2020]. British Columbia's saline lakes provide a unique opportunity to investigate the salt hydrate dynamics within diverse natural ice-brine systems, including salt hydrate precipitation in a saturating reservoir and the presence and geochemical dynamics of salt hydrates in diverse ices. Such results

can be leveraged as benchmarks for more accurate models hoping to include the geochemical and thermophysical dynamics of ternary ice-brine-hydrate systems.

5. Conclusion

The hypersaline lakes of British Columbia's Cariboo Plateau provide an exceptional terrestrial analog for planetary ice-brine systems. The range of lake chemistries and concentrations, coupled with intense winters, produces a compositionally diverse spectrum of lake ice covers. The novel observations resulting from these field expeditions expands our understanding of the biogeochemistry of relatively understudied, but broadly applicable, terrestrial analog systems, as ice-brine environments are likely ubiquitous throughout the solar system (e.g., Mars, Europa, Enceladus, etc.). Moreover, this study provides a methodology for quantifying the habitability of planetary ices that can be utilized to inform upcoming astrobiology mission planning and data analysis.

Our investigations provide insight into the relationships between both the bioburden and ionic composition of chemically diverse ices, their formation history, and their underlying parent fluid properties. This is most evident in the depth dependent trends of biological entrainment, ion entrainment, and permeability. Our results show that the characteristics of these salt rich lake ices follow similar trends to those observed in sea ice, which suggests that material entrainment is **1)** inversely proportional to thermal gradients at the ice-ocean/brine interface (equivalently ice thickness), **2)** proportional to the concentration of the parent ocean/brine reservoir and **3)** depends critically on the dynamics occurring in the gradient-rich multiphase layer near the base of the ice cover [*Buffo et al.*, 2018; *Eicken*, 1992; *Golden et al.*, 2007; *Hunke et al.*, 2011; *Nakawo and Sinha*, 1981; *Notz and Worster*, 2008]. Effectively, this work suggests that the physical mechanisms that govern the fractionation of liquids, solids, and biota within diverse ices are similar yet dependent on composition. Such a result implies that infusion of these dynamics into models of planetary ice processes and analysis of planetary data sets is well founded. Additionally, we observed a number of novel features in naturally occurring ice-brine environments that have important geophysical and astrobiological implications for both terrestrial and planetary cryohydrologic systems; these include internal brine layers in the ice cover of Basque Lake 2, widespread and heterogeneous salt hydrate precipitation and the associated effects of their latent heat of fusion on brine longevity and resistance to solidification, and the likely supercooling of brines in a natural setting.

Future work will utilize the collected profiles to validate reactive transport models of planetary ice formation and evolution (e.g. [*Brown et al.*, 2020b; *Buffo et al.*, *2020*]) that seek to simulate the thermal and physicochemical properties of diverse ice-brine systems. Physicochemical heterogeneities likely play an important role in ice shell geophysical processes [*Barr and McKinnon*, 2007; *Johnson et al.*, 2017; *Pappalardo and Barr*, 2004; *Schmidt et al.*, 2011] and proliferous biological communities are sustained by physical and thermochemical gradients in terrestrial ice-ocean/brine environments [*Daly et al.*, 2013; *Loose et al.*, 2011]. As such, devising methods and models which quantify the thermophysical, biological, and geochemical properties and dynamics of planetary ices has implications for constraining the geophysics of icy worlds and assessing the spatiotemporal habitability of their ice-brine systems.

This study is of particular importance due to the presence of magnesium sulfate and sodium carbonate in the ice. With potentially similar ice chemistries existing on a number of high-priority astrobiology targets (Mars, Europa, Enceladus), constraining the characteristics and evolution of these analog ice-brine systems has direct implications for relating spacecraft observations of surface and ice shell properties to interior ocean/brine properties, as this relies heavily on

quantifying the efficiency with which impurities are entrained and transported within the ice shell. With any potential ocean-derived biosignatures subject to similar transport processes, impurity entrainment estimates feed forward into detection limit requirements of any future ice-ocean world surface missions. The empirical data set presented here provides a unique benchmark to validate geophysical and biogeochemical models of planetary ices, a crucial tool in forecasting the dynamics, properties, and habitability of ice-ocean worlds. With a number of upcoming ice-ocean world missions promising to return observations with orders of magnitude higher spatial and spectral resolution than their predecessors and more in situ techniques, leveraging terrestrial analog systems such as British Columbia's hypersaline lakes can provide useful guides for the interpretation of data by linking measurements of ice composition to its thermodynamic history, parent fluid properties, and habitability.

Author Contribution Statement

JJB aided in the collection and analysis of all samples and field measurements, carried out PHREEQC simulations, and lead the writing and editing of the manuscript. EKB aided in the collection and analysis of all samples and field measurements and participated in writing and editing the manuscript. AP provided logistical support for the field work in 2019, aided in the collection and analysis of all samples and field measurements and participated in writing and editing the manuscript. BES aided in the analysis of all samples and field measurements, assisted in planning field work methods and participated in writing and editing the manuscript. BK aided in the flow cytometry analysis of the field samples and participated in writing and editing the manuscript. JL aided in the analysis of all samples and field measurements, assisted in planning field work methods and participated in writing and editing the manuscript. JB aided in the flow cytometry analysis of the field samples, assisted in planning field work methods and participated in writing and editing the manuscript. MG aided in the ionic composition analysis of samples, assisted in planning field work methods and participated in editing the manuscript. JBG aided in the fluorescence microscopy analysis of samples, assisted in planning field work methods and participated in editing the manuscript. TP aided in the analysis of field samples. CC aided in the writing of the porosity and permeability sections of the manuscript. PD aided in the collection of sample and field measurements.

Author Disclosure Statement

The authors declare no personal, financial, funding, employment, or other competing interests exist.

Funding Statement

JJB, EKB, AP, BES, BK, JL, JB, JBG, and PD were funded by the NASA Network for Life Detection project Oceans Across Space and Time (Grant Number: 80NSSC18K1301). JJB and EKB were additionally funded through an American Philosophical Society Lewis and Clark Fund for Exploration and Field Research in Astrobiology grant (Title: *Biosignature Dynamics in British Columbia's Frozen Hypersaline Lakes: Implications for the Habitability and Bioburden of Ice-Brine Environments*). AP was also supported by NASA Exobiology grant, *Biosignature Preservation in Sulfate Dominated Environments* (Grant Number: 80NSSC20K0849).

6. References

824 Ackley, S. F., and C. W. Sullivan (1994), Physical Controls on the Development and
825 Characteristics of Antarctic Sea-Ice Biological Communities - a Review and Synthesis,
826 *Deep-Sea Research Part I-Oceanographic Research Papers*, *41*(10), 1583-1604, doi:Doi
827 10.1016/0967-0637(94)90062-0.
828 Barr, A. C., and W. B. McKinnon (2007), Convection in ice I shells and mantles with self-
829 consistent grain size, *Journal of Geophysical Research: Planets*, *112*(E2),
830 doi:10.1029/2006JE002781.
831 Bauer, J. M., B. J. Buratti, J. Y. Li, J. A. Mosher, M. D. Hicks, B. E. Schmidt, and J. D. Goguen
832 (2010), Direct Detection of Seasonal Changes on Triton with Hubble Space Telescope,
833 *Astrophysical Journal Letters*, *723*(1), L49-L52, doi:10.1088/2041-8205/723/1/L49.
834 Bear, J. (2013), *Dynamics of fluids in porous media*, Courier Corporation.
835 Brown, E., J. Buffo, M. Grantham, A. Pontefract, J. Glass, E. Ingall, P. Doran, M. Toubes-Rodrigo,
836 H. Dion-Kirschner, and C. Carr (2020a), Trapped in the Ice: An Analysis of Brines in
837 British Columbia's Hypersaline Lakes, *LPI*(2326), 2218.
838 Brown, E. K., et al. (2020b), TRAPPED IN THE ICE: AN ANALYSIS OF BRINES IN BRITISH
839 COLUMBIA'S HYPERSALINE LAKES, in *Lunar and Planetary Science Conference*,
840 edited, Woodlands, TX.
841 Buffo, J., B. Schmidt, C. Huber, and C. Meyer (2021a), Characterizing the Ice-Ocean Interface of
842 Icy Worlds: A Theoretical Approach, *Icarus*.
843 Buffo, J., B. Schmidt, C. Huber, and C. Walker (*2020*), Entrainment and dynamics of ocean-
844 derived impurities within Europa's ice shell, *JGR: Planets*.
845 Buffo, J., B. Schmidt, A. Pontefract, and J. Lawrence (2019), Frozen Fingerprints: Chemical and
846 Biological Entrainment in Planetary Ices, in *Astrobiology Science Conference*, edited,
847 Bellevue, Washington.
848 Buffo, J. J. (2019), Multiphase reactive transport in planetary ices, Georgia Institute of
849 Technology.
850 Buffo, J. J., C. R. Meyer, J. R. Parkinson, and B. E. Schmidt (2021b), Dynamics of a solidifying
851 icy satellite shell, *JGR: Planets*.
852 Buffo, J. J., B. E. Schmidt, and C. Huber (2018), Multiphase Reactive Transport and Platelet Ice
853 Accretion in the Sea Ice of McMurdo Sound, Antarctica, *Journal of Geophysical Research-*
854 *Oceans*, *123*(1), 324-345, doi:10.1002/2017jc013345.
855 Čadek, O., G. Tobie, T. Van Hoolst, M. Massé, G. Choblet, A. Lefèvre, G. Mitri, R. M. Baland,
856 M. Běhounková, and O. Bourgeois (2016), Enceladus's internal ocean and ice shell
857 constrained from Cassini gravity, shape, and libration data, *Geophysical Research Letters*,
858 *43*(11), 5653-5660.
859 Carr, M. H. (1987), Water on Mars, *Nature*, *326*(6108), 30-35, doi:DOI 10.1038/326030a0.
860 Chivers, C., J. Buffo, and B. Schmidt (2021), Thermal and Chemical Evolution of Small, Shallow
861 Water Bodies on Europa, *JGR: Planets*(2326), 1047.
862 Colangelo-Lillis, J., H. Eicken, S. Carpenter, and J. Deming (2016), Evidence for marine origin
863 and microbial-viral habitability of sub-zero hypersaline aqueous inclusions within
864 permafrost near Barrow, Alaska, *FEMS Microbiology Ecology*, *92*(5), fiw053.
865 Cosciotti, B., A. Balbi, A. Ceccarelli, C. Fagliarone, E. Mattei, S. E. Lauro, F. Di Paolo, E.
866 Pettinelli, and D. Billi (2019), Survivability of Anhydrobiotic Cyanobacteria in Salty Ice:
867 Implications for the Habitability of Icy Worlds, *Life (Basel)*, *9*(4), 86,
868 doi:10.3390/life9040086.

869 Cottier, F., H. Eicken, and P. Wadhams (1999), Linkages between salinity and brine channel
870 distribution in young sea ice, *Journal of Geophysical Research-Oceans*, *104*(C7), 15859-
871 15871, doi:Doi 10.1029/1999jc900128.
872 Cox, G. F., and W. F. Weeks (1974), Salinity variations in sea ice, *Journal of Glaciology*, *13*(67),
873 109-120.
874 Craft, K. L., G. W. Patterson, R. P. Lowell, and L. Germanovich (2016), Fracturing and flow:
875 Investigations on the formation of shallow water sills on Europa, *Icarus*, *274*, 297-313,
876 doi:10.1016/j.icarus.2016.01.023.
877 Daly, M., F. Rack, and R. Zook (2013), Edwardsiella andrillae, a new species of sea anemone from
878 Antarctic ice, *PLoS One*, *8*(12), e83476, doi:10.1371/journal.pone.0083476.
879 Di Paolo, F., S. E. Lauro, D. Castelletti, G. Mitri, F. Bovolo, B. Cosciotti, E. Mattei, R. Orosei, C.
880 Notarnicola, and L. Bruzzone (2016), Radar signal penetration and horizons detection on
881 Europa through numerical simulations, *IEEE Journal of Selected Topics in Applied Earth*
882 *Observations and Remote Sensing*, *10*(1), 118-129.
883 Doran, P. T., C. H. Fritsen, C. P. McKay, J. C. Priscu, and E. E. Adams (2003), Formation and
884 character of an ancient 19-m ice cover and underlying trapped brine in an "ice-sealed" east
885 Antarctic lake, *Proc Natl Acad Sci U S A*, *100*(1), 26-31, doi:10.1073/pnas.222680999.
886 Durham, W. B., L. A. Stern, T. Kubo, and S. H. Kirby (2005), Flow strength of highly hydrated
887 Mg-and Na-sulfate hydrate salts, pure and in mixtures with water ice, with application to
888 Europa, *Journal of Geophysical Research: Planets*, *110*(E12).
889 Eicken, H. (1992), Salinity Profiles of Antarctic Sea Ice - Field Data and Model Results, *Journal*
890 *of Geophysical Research-Oceans*, *97*(C10), 15545-15557, doi:Doi 10.1029/92jc01588.
891 Ellis, B., P. Haaland, F. Hahne, N. Le Meur, N. Gopalakrishnan, J. Spidlen, M. Jiang, and G. Finak
892 (2009), flowCore: Basic structures for flow cytometry data, *R package version*, *1*(0).
893 Fanale, F. P., J. C. Granahan, T. B. McCord, G. Hansen, C. A. Hibbitts, R. Carlson, D. Matson, A.
894 Ocampo, L. Kamp, and W. Smythe (1999), Galileo's multiinstrument spectral view of
895 Europa's surface composition, *Icarus*, *139*(2), 179-188.
896 Fastook, J. L., and J. W. Head (2015), Glaciation in the Late Noachian Icy Highlands: Ice
897 accumulation, distribution, flow rates, basal melting, and top-down melting rates and
898 patterns, *Planetary and Space Science*, *106*, 82-98, doi:10.1016/j.pss.2014.11.028.
899 Fastook, J. L., J. W. Head, D. R. Marchant, F. Forget, and J.-B. Madeleine (2012), Early Mars
900 climate near the Noachian–Hesperian boundary: Independent evidence for cold conditions
901 from basal melting of the south polar ice sheet (Dorsa Argentea Formation) and
902 implications for valley network formation, *Icarus*, *219*(1), 25-40.
903 Feltham, D. L., N. Untersteiner, J. S. Wettlaufer, and M. G. Worster (2006), Sea ice is a mushy
904 layer, *Geophysical Research Letters*, *33*(14), doi:Artn L14501
905 10.1029/2006gl026290.
906 Fisher, L. A., A. Pontefract, S. Som, C. E. Carr, B. Klempay, B. Schmidt, J. Bowman, and D. H.
907 Bartlett (2021), Current state of athalassohaline deep sea hypersaline anoxic basin (DHAB)
908 research–recommendations for future work and relevance to astrobiology, *Environmental*
909 *Microbiology*.
910 Foster, I. S., P. L. King, B. C. Hyde, and G. Southam (2010), Characterization of halophiles in
911 natural MgSO4 salts and laboratory enrichment samples: astrobiological implications for
912 Mars, *Planetary and Space Science*, *58*(4), 599-615.

Fox-Powell, M. G., and C. S. Cockell (2018), Building a Geochemical View of Microbial Salt Tolerance: Halophilic Adaptation of Marinococcus in a Natural Magnesium Sulfate Brine, *Front Microbiol*, *9*, 739, doi:10.3389/fmicb.2018.00739.

Fox-Powell, M. G., J. E. Hallsworth, C. R. Cousins, and C. S. Cockell (2016), Ionic Strength Is a Barrier to the Habitability of Mars, *Astrobiology*, *16*(6), 427-442, doi:10.1089/ast.2015.1432.

Fox-Powell, M. G., R. Hamp, S. P. Schwenzer, K. Olsson-Francis, V. K. Pearson, and C. R. Cousins (2020), Phase fractionation and the fate of bioessential elements during freezing of simulated Enceladus ocean fluids, in *AGU Fall Meeting*, edited.

Fox-Powell, M. G., and C. Cousins (2021), Partitioning of crystalline and amorphous phases during freezing of simulated Enceladus ocean fluids, *Journal of Geophysical Research: Planets*, e2020JE006628.

Freitag, J., and H. Eicken (2003), Meltwater circulation and permeability of Arctic summer sea ice derived from hydrological field experiments, *Journal of Glaciology*, *49*(166), 349-358, doi:Doi 10.3189/172756503781830601.

Gilichinsky, D., E. Rivkina, C. Bakermans, V. Shcherbakova, L. Petrovskaya, S. Ozerskaya, N. Ivanushkina, G. Kochkina, K. Laurinavichuis, and S. Pecheritsina (2005), Biodiversity of cryopegs in permafrost, *FEMS microbiology ecology*, *53*(1), 117-128.

Gilichinsky, D., E. Rivkina, V. Shcherbakova, K. Laurinavichuis, and J. Tiedje (2003), Supercooled water brines within permafrost—an unknown ecological niche for microorganisms: a model for astrobiology, *Astrobiology*, *3*(2), 331-341.

Glein, C. R., J. A. Baross, and J. H. Waite (2015), The pH of Enceladus' ocean, *Geochimica Et Cosmochimica Acta*, *162*, 202-219, doi:10.1016/j.gca.2015.04.017.

Golden, K. M., S. F. Ackley, and V. V. Lytle (1998), The percolation phase transition in sea Ice, *Science*, *282*(5397), 2238-2241, doi:10.1126/science.282.5397.2238.

Golden, K. M., H. Eicken, A. L. Heaton, J. Miner, D. J. Pringle, and J. Zhu (2007), Thermal evolution of permeability and microstructure in sea ice, *Geophysical Research Letters*, *34*(16), doi:Artn L16501
10.1029/2007gl030447.

Grau Galofre, A., A. M. Jellinek, and G. R. Osinski (2020), Valley formation on early Mars by subglacial and fluvial erosion, *Nature Geoscience*, 1-6.

Grevel, K.-D., J. Majzlan, A. Benisek, E. Dachs, M. Steiger, A. D. Fortes, and B. Marler (2012), Experimentally determined standard thermodynamic properties of synthetic MgSO4· 4H2O (starkeyite) and MgSO4· 3H2O: A revised internally consistent thermodynamic data set for magnesium sulfate hydrates, *Astrobiology*, *12*(11), 1042-1054.

Hallsworth, J. E., et al. (2007), Limits of life in MgCl2-containing environments: chaotropicity defines the window, *Environ Microbiol*, *9*(3), 801-813, doi:10.1111/j.1462-2920.2006.01212.x.

Hammond, N. P., E. Parmenteir, and A. C. Barr (2018), Compaction and Melt Transport in Ammonia-Rich Ice Shells: Implications for the Evolution of Triton, *Journal of Geophysical Research: Planets*, *123*(12), 3105-3118.

Han, L., and A. P. Showman (2005), Thermo-compositional convection in Europa's icy shell with salinity, *Geophysical research letters*, *32*(20).

Howell, S. M., and R. T. Pappalardo (2018), Band formation and ocean-surface interaction on Europa and Ganymede, *Geophysical Research Letters*, *45*(10), 4701-4709.

Howell, S. M., and R. T. Pappalardo (2020), NASA's Europa Clipper-a mission to a potentially habitable ocean world, *Nat Commun*, *11*(1), 1311, doi:10.1038/s41467-020-15160-9.

Hunke, E. C., D. Notz, A. K. Turner, and M. Vancoppenolle (2011), The multiphase physics of sea ice: a review for model developers, *Cryosphere*, *5*(4), 989-1009, doi:10.5194/tc-5-989-2011.

Iwahana, G., Z. S. Cooper, S. D. Carpenter, J. W. Deming, and H. Eicken (2021), Intra-ice and intra-sediment cryopeg brine occurrence in permafrost near Utqiaġvik (Barrow), *Permafrost and Periglacial Processes*.

Jenkins, O. P. (1918), Spotted lakes of epsomite in Washington and British Columbia, *American Journal of Science*, *46*(275), 638-644.

Johnson, B. C., R. Y. Sheppard, A. C. Pascuzzo, E. A. Fisher, and S. E. Wiggins (2017), Porosity and Salt Content Determine if Subduction Can Occur in Europa's Ice Shell, *Journal of Geophysical Research-Planets*, *122*(12), 2765-2778, doi:10.1002/2017je005370.

Journaux, B., J. M. Brown, A. Pakhomova, I. E. Collings, S. Petitgirard, P. Espinoza, T. Boffa Ballaran, S. D. Vance, J. Ott, and F. Cova (2020), Holistic Approach for Studying Planetary Hydrospheres: Gibbs Representation of Ices Thermodynamics, Elasticity, and the Water Phase Diagram to 2,300 MPa, *Journal of Geophysical Research: Planets*, *125*(1), e2019JE006176.

Kalousova, K., D. M. Schroeder, and K. M. Soderlund (2017), Radar attenuation in Europa's ice shell: Obstacles and opportunities for constraining the shell thickness and its thermal structure, *Journal of Geophysical Research-Planets*, *122*(3), 524-545, doi:10.1002/2016je005110.

Kargel, J. S., J. Z. Kaye, J. W. Head, G. M. Marion, R. Sassen, J. K. Crowley, O. Prieto Ballesteros, S. A. Grant, and D. L. Hogenboom (2000), Europa's crust and ocean: Origin, composition, and the prospects for life, *Icarus*, *148*(1), 226-265, doi:10.1006/icar.2000.6471.

Klempay, B., N. Arandia-Gorostidi, A. E. Dekas, D. H. Bartlett, C. E. Carr, P. T. Doran, A. Dutta, N. Erazo, L. A. Fisher, and J. B. Glass (2021), Microbial diversity and activity in Southern California salterns and bitterns: analogues for remnant ocean worlds, *Environmental Microbiology*.

Lauro, S. E., et al. (2020), Multiple subglacial water bodies below the south pole of Mars unveiled by new MARSIS data, *Nature Astronomy*, doi:10.1038/s41550-020-1200-6.

Loose, B., L. A. Miller, S. Elliott, and T. Papakyriakou (2011), Sea Ice Biogeochemistry and Material Transport Across the Frozen Interface, *Oceanography*, *24*(3), 202-218, doi:DOI 10.5670/oceanog.2011.72.

Malmgren, F. (1927), *On the properties of sea-ice*, AS John Griegs Boktrykkeri.

Marion, G., R. Farren, and A. Komrowski (1999), Alternative pathways for seawater freezing, *Cold Regions Science and Technology*, *29*(3), 259-266.

Marion, G. M., C. H. Fritsen, H. Eicken, and M. C. Payne (2003), The search for life on Europa: limiting environmental factors, potential habitats, and Earth analogues, *Astrobiology*, *3*(4), 785-811, doi:10.1089/153110703322736105.

Maus, S., M. Schneebeli, and A. Wiegmann (2020), An X-ray micro-tomographic study of the pore space, permeability and percolation threshold of young sea ice, *The Cryosphere Discussions*, 1-30.

McCarthy, C., R. F. Cooper, D. L. Goldsby, W. B. Durham, and S. H. Kirby (2011), Transient and steady state creep response of ice I and magnesium sulfate hydrate eutectic aggregates, *Journal of Geophysical Research-Planets*, *116*(E4), doi:Artn E04007

10.1029/2010je003689.
McKenzie, D. (1989), Some remarks on the movement of small melt fractions in the mantle, *Earth and planetary science letters*, *95*(1-2), 53-72.
McKinnon, W. B. (1999), Convective instability in Europa's floating ice shell, *Geophysical Research Letters*, *26*(7), 951-954, doi:Doi 10.1029/1999gl900125.
Michaut, C., and M. Manga (2014), Domes, pits, and small chaos on Europa produced by water sills, *Journal of Geophysical Research: Planets*, *119*(3), 550-573.
Murray, A. E., et al. (2012), Microbial life at -13 degrees C in the brine of an ice-sealed Antarctic lake, *Proceedings of the National Academy of Sciences of the United States of America*, *109*(50), 20626-20631, doi:10.1073/pnas.1208607109.
Nakawo, M., and N. K. Sinha (1981), Growth rate and salinity profile of first-year sea ice in the high Arctic, *Journal of Glaciology*, *27*(96), 315-330.
Nathan, E., M. Berton, T. Girona, H. Karani, C. Huber, J. Head III, and P. Williard (2019), The Freezing and Fracture of Icy Satellites: Experimental Analog and Stress Analysis, *AGUFM*, *2019*, P53D-3489.
Nimmo, F., and R. T. Pappalardo (2006), Diapir-induced reorientation of Saturn's moon Enceladus, *Nature*, *441*(7093), 614-616, doi:10.1038/nature04821.
Nimmo, F., and P. Schenk (2006), Normal faulting on Europa: implications for ice shell properties, *Journal of Structural Geology*, *28*(12), 2194-2203, doi:10.1016/j.jsg.2005.08.009.
Notz, D., and M. G. Worster (2008), In situ measurements of the evolution of young sea ice, *Journal of Geophysical Research-Oceans*, *113*(C3), doi:Artn C03001
10.1029/2007jc004333.
Notz, D., and M. G. Worster (2009), Desalination processes of sea ice revisited, *Journal of Geophysical Research-Oceans*, *114*(C5), doi:Artn C05006
10.1029/2008jc004885.
Ojha, L., J. Buffo, S. Karunatillake, and M. Siegler (*2020*), Groundwater Production from Geothermal Heating on Early Mars and Implications for Early Matian Habitability, *Science advances*.
Ojha, L., M. B. Wilhelm, S. L. Murchie, A. S. McEwen, J. J. Wray, J. Hanley, M. Massé, and M. Chojnacki (2015), Spectral evidence for hydrated salts in recurring slope lineae on Mars, *Nature Geoscience*, *8*(11), 829.
Oren, A. (2013), Life in magnesium-and calcium-rich hypersaline environments: salt stress by chaotropic ions, in *Polyextremophiles*, edited, pp. 215-232, Springer.
Orosei, R., et al. (2018), Radar evidence of subglacial liquid water on Mars, *Science*, *361*(6401), 490-493, doi:10.1126/science.aar7268.
Pappalardo, R. T., and A. C. Barr (2004), The origin of domes on Europa: The role of thermally induced compositional diapirism, *Geophysical Research Letters*, *31*(1), doi:Artn L01701
10.1029/2003gl019202.
Parkhurst, D. L., and C. Appelo (1999), User's guide to PHREEQC (Version 2): A computer program for speciation, batch-reaction, one-dimensional transport, and inverse geochemical calculations, *Water-resources investigations report*, *99*(4259), 312.
Parkhurst, D. L., and C. Appelo (2013), Description of input and examples for PHREEQC version 3: a computer program for speciation, batch-reaction, one-dimensional transport, and inverse geochemical calculations*Rep. 2328-7055*, US Geological Survey.

Parkinson, C. D., M. C. Liang, Y. L. Yung, and J. L. Kirschivnk (2008), Habitability of enceladus: planetary conditions for life, *Orig Life Evol Biosph*, *38*(4), 355-369, doi:10.1007/s11084-008-9135-4.

Peterson, R. A., and W. B. Krantz (2008), Differential frost heave model for patterned ground formation: Corroboration with observations along a North American arctic transect, *Journal of Geophysical Research-Biogeosciences*, *113*(G3), doi:Artn G03s04 10.1029/2007jg000559.

Pontefract, A., C. E. Carr, and M. R. Osburn (2019), The Role of Ionic Composition and Concentration on Biosignature Preservation: Lessons from the "Spotted" Lakes of British Colombia, paper presented at 2019 Astrobiology Science Conference, AGU.

Pontefract, A., T. F. Zhu, V. K. Walker, H. Hepburn, C. Lui, M. T. Zuber, G. Ruvkun, and C. E. Carr (2017), Microbial Diversity in a Hypersaline Sulfate Lake: A Terrestrial Analog of Ancient Mars, *Front Microbiol*, *8*, 1819, doi:10.3389/fmicb.2017.01819.

Priscu, J. C., C. H. Fritsen, E. E. Adams, S. J. Giovannoni, H. W. Paerl, C. P. McKay, P. T. Doran, D. A. Gordon, B. D. Lanoil, and J. L. Pinckney (1998), Perennial Antarctic lake ice: an oasis for life in a polar desert, *Science*, *280*(5372), 2095-2098, doi:10.1126/science.280.5372.2095.

Priscu, J. C., and K. P. Hand (2012), Microbial habitability of icy worlds, *Microbe*, *7*(4), 167-172.

Rapin, W., et al. (2019), An interval of high salinity in ancient Gale crater lake on Mars, *Nature Geoscience*, *12*(11), 889-+, doi:10.1038/s41561-019-0458-8.

Renaut, R. W., and P. R. Long (1989), Sedimentology of the Saline Lakes of the Cariboo Plateau, Interior British-Columbia, Canada, *Sedimentary Geology*, *64*(4), 239-264, doi:Doi 10.1016/0037-0738(89)90051-1.

Rutishauser, A., D. D. Blankenship, M. Sharp, M. L. Skidmore, J. S. Greenbaum, C. Grima, D. M. Schroeder, J. A. Dowdeswell, and D. A. Young (2018), Discovery of a hypersaline subglacial lake complex beneath Devon Ice Cap, Canadian Arctic, *Sci Adv*, *4*(4), eaar4353, doi:10.1126/sciadv.aar4353.

Santibáñez, P. A., A. B. Michaud, T. J. Vick-Majors, J. D'Andrilli, A. Chiuchiolo, K. P. Hand, and J. C. Priscu (2019), Differential Incorporation of Bacteria, Organic Matter, and Inorganic Ions into Lake Ice during Ice Formation, *Journal of Geophysical Research: Biogeosciences*.

Schmidt, B. (2020), The Astrobiology of Europa and the Jovian System, *Planetary Astrobiology*, 185.

Schmidt, B. E., D. D. Blankenship, G. W. Patterson, and P. M. Schenk (2011), Active formation of 'chaos terrain' over shallow subsurface water on Europa, *Nature*, *479*(7374), 502-505, doi:10.1038/nature10608.

Schmidt, B. E., J. Buffo, and A. Main Campus (2017), Biomarker Production and Preservation on Europa, paper presented at European Planetary Science Congress.

Shimanov, A., I. Komarov, and T. Kireeva (2020), Peculiarities of the changes in chemical composition of cryopegs of the Yamal Peninsula during cryogenic concentration, *Moscow University Geology Bulletin*, *75*, 72-79.

Sori, M. M., and A. M. Bramson (2019), Water on Mars, with a grain of salt: local heat anomalies are required for basal melting of ice at the South pole today, *Geophysical Research Letters*, *46*(3), 1222-1231.

Sotin, C., and G. Tobie (2004), Internal structure and dynamics of the large icy satellites, *Comptes Rendus Physique*, *5*(7), 769-780, doi:10.1016/j.crhy.2004.08.001.

Sparks, W. B., K. P. Hand, M. A. McGrath, E. Bergeron, M. Cracraft, and S. E. Deustua (2016), Probing for Evidence of Plumes on Europa with Hst/Stis, *Astrophysical Journal*, *829*(2), 121, doi:Artn 121
10.3847/0004-637x/829/2/121.
Spindler, M. (1994), Notes on the Biology of Sea-Ice in the Arctic and Antarctic, *Polar Biology*, *14*(5), 319-324.
Srivastava, A., V. K. Pearson, S. P. Schwenzer, M. Macey, M. Toubes-Rodrigo, T. J. McGenity, A. Pontefract, and K. Olsson-Francis (2021), Are Sulfates the Viable Substrates for the Long-Term Preservation of Lipids on Mars?, in *LPSC*, edited.
Stevens, A. H., and C. S. Cockell (2020), A Systematic Study of the Limits of Life in Mixed Ion Solutions: Physicochemical Parameters Do Not Predict Habitability, *Frontiers in Microbiology*, *11*, 1478.
Tedesco, L., and M. Vichi (2014), Sea ice biogeochemistry: a guide for modellers, *PLoS One*, *9*(2), e89217, doi:10.1371/journal.pone.0089217.
Thomas, D. N., and G. S. Dieckmann (2003), Biogeochemistry of Antarctic sea ice, in *Oceanography and Marine Biology, An Annual Review, Volume 40*, edited, pp. 151-156, CRC Press.
Toner, J. D., D. C. Catling, and B. Light (2014), The formation of supercooled brines, viscous liquids, and low-temperature perchlorate glasses in aqueous solutions relevant to Mars, *Icarus*, *233*, 36-47, doi:10.1016/j.icarus.2014.01.018.
Tosca, N. J., A. H. Knoll, and S. M. McLennan (2008), Water activity and the challenge for life on early Mars, *Science*, *320*(5880), 1204-1207, doi:10.1126/science.1155432.
Vance, S. D., B. Journaux, M. Hesse, and G. Steinbrügge (2020), The Salty Secrets of Icy Ocean Worlds, *Journal of Geophysical Research: Planets*, e2020JE006736.
Vaniman, D. T., D. L. Bish, S. J. Chipera, C. I. Fialips, J. W. Carey, and W. C. Feldman (2004), Magnesium sulphate salts and the history of water on Mars, *Nature*, *431*(7009), 663-665, doi:10.1038/nature02973.
Walker, C., B. Schmidt, and J. Bassis (2014), Breaking the ice: On the application of fracture system mechanics and fragmentation theory to the chaos regions of Europa, *LPI*(1777), 2659.
Weeks, W. F., and S. F. Ackley (1986), The growth, structure, and properties of sea ice, in *The geophysics of sea ice*, edited, pp. 9-164, Springer.
Weller, M. B., L. Fuchs, T. W. Becker, and K. M. Soderlund (2019), Convection in Thin Shells of Icy Satellites: Effects of Latitudinal Surface Temperature Variations, *Journal of Geophysical Research-Planets*, *124*(8), 2029-2053, doi:10.1029/2018je005799.
Wray, J., R. Milliken, C. M. Dundas, G. A. Swayze, J. Andrews-Hanna, A. Baldridge, M. Chojnacki, J. Bishop, B. Ehlmann, and S. L. Murchie (2011), Columbus crater and other possible groundwater-fed paleolakes of Terra Sirenum, Mars, *Journal of Geophysical Research: Planets*, *116*(E1).
Zolotov, M. Y. (2007), An oceanic composition on early and today's Enceladus, *Geophysical Research Letters*, *34*(23), doi:Artn L23203
10.1029/2007gl031234.
Zolotov, M. Y., and E. L. Shock (2001), Composition and stability of salts on the surface of Europa and their oceanic origin, *Journal of Geophysical Research-Planets*, *106*(E12), 32815-32827, doi:Doi 10.1029/2000je001413.

Zorzano, M. P., E. Mateo-Marti, O. Prieto-Ballesteros, S. Osuna, and N. Renno (2009), Stability of liquid saline water on present day Mars, *Geophysical Research Letters*, *36*(20), doi:Artn L20201
10.1029/2009gl040315.

Supplementary Material

S1 - Flow Cytometry Methods and Description of Fluorescence Microscopy Work

Cell densities from samples collected in February 2019 were quantified using flow cytometry adhering to the methods found in [*Webb et al.*, 2019] and *[Klempay et al., 2021]*. Prior to analysis, the samples meant for biological analysis were treated with 2.5% glutaraldehyde solution to fix the cells (for a final glutaraldehyde concentration of 0.25%) and placed in a -20C freezer before finally being shipped frozen to Scripps Institution of Oceanography. Fixed samples were stained with SYBR Green I nucleic acid dye (Molecular Probes) and spiked with a known quantity of 123count eBeads counting beads (Thermo Fisher). Samples were then run on a Guava easyCyte HT flow cytometer (Luminex). Flow cytometry outputs were analyzed in R using the flowCore library [*Ellis et al.*, 2009] and custom scripts [*Klempay et al.*, 2021]. To confirm results, duplicate samples from 2019 were also analyzed using fluorescence microscopy (Figure S1). Cells were stained with 4′,6-diamidino-2-phenylindole (DAPI) and imaged using a Zeiss Epifluorescent Microscope. Images were acquired (e.g. Figure S1a-c) and analyzed using the edge detection algorithms of Fiji (ImageJ) software. The range of cell densities (on the order of 10^6 cells/ml) from both fluorescent microscopy and FCM counting methods are consistent with each other and are similar to the values found using flow cytometry analysis on the February 2020 samples (Section 3.4 & Figure 9).

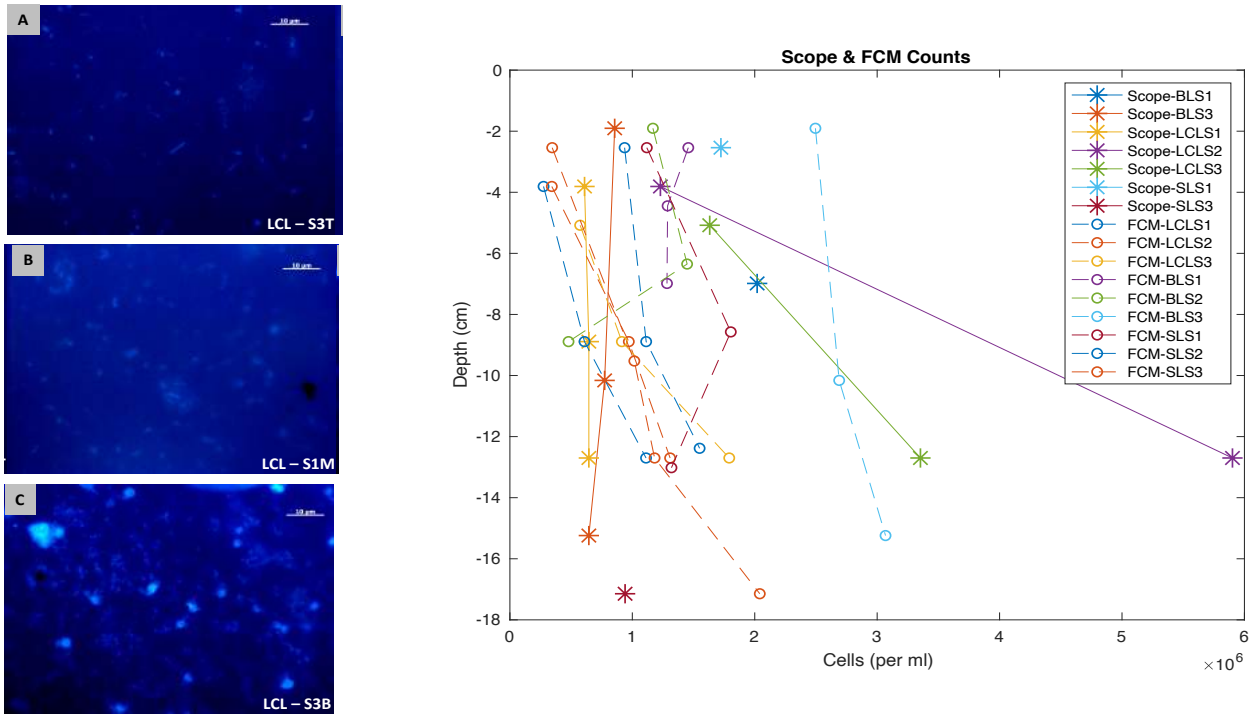

Figure S1. Fluorescent microscopy and flow cytometry cell density estimates (February 2019 samples). **A-C)** Fluorescent microscopy images of Last Chance Lake samples, showing the increasing abundance of organisms with depth. **Right)** Fluorescent microscopy ('Scope') and flow cytometry ('FCM') cell density estimates for February 2019 samples. Value and trends observed in the 2019 FCM counts are similar to those from the 2020 samples (e.g. increasing cell densities with depth, cell densities ~10^6 cells/ml). Inversions between the -6 cm and -9 cm layers can also be seen in both the plots (See Figure 9) for Basque Lake 2 – Site 2. Generally, the FCM and flow cytometry data both have values that fall in the range of $\sim 0.5x10^6$ to $\sim 2.0x10^6$.

Figure S2. Image of salt hydrates excavated from Last Chance Lake during the recovery of the HOBO temperature sensors during the February 2020 field season – hammer for size reference.

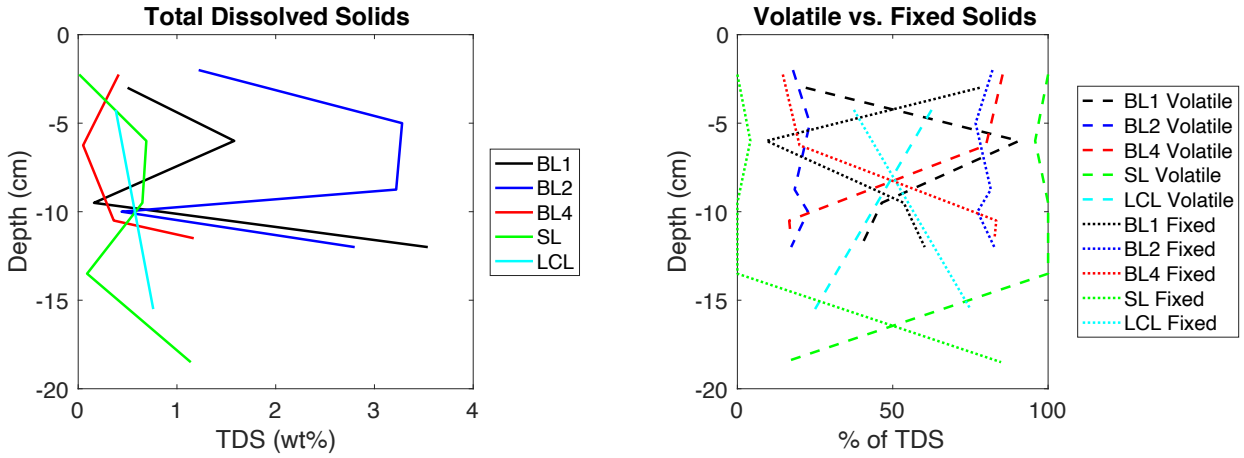

Figure S3. Left) Total dissolved solids (TDS) for the February 2020 samples expressed in a percentage of weight. As expected, trends follow the ion profiles for the lakes (Figure 9). **Right)** Volatile solids (organic material) and fixed solids (inorganic material) plotted as a percentage of the TDS for the respective sample.

Lake Site	Depth Below Surface (cm)	Temp-erature (C)	Alkalinity as CaCO3 (mg/L)	Cl (ppm)	SO4 (ppm)	Ca (mg/kg)	Mg (mg/kg)	K (mg/kg)	Na (mg/kg)	Conductivity (µS/cm)	pH	Total Dissolved Solids (wt%)	Volatile Solids (wt%)	Fixed Solids (wt%)
BL1-S1T	3	-3.54	560	270	30100	210	6750	<210	2510	3,900	10.11	0.5	22	78
BL1-S1M	6	-3.52	190	<250	7940	130	1580	<210	660	1,350	9.84	1.58	90.65	9.35
BL1-S1B	10.5	-3.38	330	<240	10470	160	2160	<210	850	1,678	9.7	0.16	36.36	63.64
BL1-S1Br	12 to 16	-2.73	2290	1430	147190	490	31410	1150	11400	1,230	10.2	3.54	39.7	60.3
BL2-S2T1	2	-4.96	380	<250	79500	150	17140	<200	3440	7,120	9.28	1.22	17.89	82.11
BL2-S2T2	5	-5.24	380	540	188390	390	41890	570	8840	13,840	9.5	3.28	23.33	76.67
BL2-S2M1	8.75	-5.15	480	560	196430	450	43720	590	9020	14,010	9.68	3.22	18.43	81.57
BL2-S2M2	10	-5.35	140	<240	26440	110	5830	<220	1160	3,300	9.18	0.44	22.73	77.27
BL2-S2Br	12 to 14	-5.11	380	550	172490	310	38590	630	9690	13,140	9.45	3	17	82.7
BL4-S1T	2.25	-2.46	90	<240	6890	<80	1280	<200	1070	1,265	9.58	0.41	85.37	14.63
BL4-S1M	6.25	-2.51	90	<240	4970	<80	830	<200	700	925	9.6	0.05	80	20
BL4-S1B	10.5		190	<250	26660	100	4510	<210	3530	3,500	9.73	0.36	16.67	83.33
BL4-S1Br	11.5 to 15	-2.46	570	460	71570	290	12850	440	9520	8,220	9.86	1.17	17.24	82.76
SLS-S1T	2.25	-2.06	90	<250	420	<80	80	<210	<210	99	9.47	0.01	<100	<0.01
SLS-S1M1	6	-1.97	90	<250	320	<80	60	<200	<200	80	9.7	0.69	95.83	4.17
SLS-S1M2	9.5	-1.93	90	<250	350	<80	70	<200	<200	87	9.86	0.65	<100	<0.01
SLS-S1B	13.5	-1.7	90	<240	4680	<80	980	<200	380	809	9.8	0.09	<100	<0.01
SLS-S1Br	18.5 to 42	-0.53	170	380	68860	270	15560	370	5000	7,180	10.43	1.14	15.13	84.87
LCL-S1T	4.25	-3.24	17080	2330	3580	<80	<40	270	11250	4390	11.4	0.38	62.5	37.5
LCL-S1Br	15.5	-2.75	46920	6560	9370	<90	<40	820	31020	10,320	11.13	0.76	25	75

Table S1. Comprehensive set of analyzed and observed data for Basque Lake 1 – Site 1 (BL1-S1x), Basque Lake 2 – Site 2 (BL2-S2x), Basque Lake 4 – Site 1 (BL4-S1x), Salt Lake – Site 1 (SL-S1x), and Last Chance Lake – Site 1 (LCL-S1x) where 'x' represents which layer of ice the sample corresponds to: top (T), middle (M), bottom (B), or brine (Br). (February 2020 data)

Sample	Cells (ml^{-1})
BL1-S1B	1386312.5
BL1-S1Br	2461574.074
BL1-S1M	1459391.892
BL1-S1T	1129100
BL1-S2B	1438961
BL1-S2Br	2291754.386
BL1-S2M	2581354.167
BL1-S2T	1765684.932
BL1-S3Br	1797812.5
BL1-S3M	1203780.488
BL1-S3T	1478181.818
BL2-S1Br	2928289.474
BL2-S1M	893588.2353
BL2-S1T	255113.6364
BL2-S2B	2045423.729
BL2-S2M1	1229210.526
BL2-S2M2	1358205.128
BL2-S2T1	1448815.789
BL2-S2T2	2503723.404
BL2-S3B	1405886.076
BL2-S3M	1749696.97
BL2-S3T	1048651.685

Sample	Cells (ml^{-1})
BL4-S1B	1515000
BL4-S1Br	1704383.562
BL4-S1M	1179930.556
BL4-S1T	940531.9149
BL4-S2Br	1990833.333
BL4-S2T	1548534.483
LCL-S1Br	1475437.5
LCL-S1T	1084466.667
ML-Br	1266379.31
SL-S1B	1599848.485
SL-S1Br	1511707.317
SL-S1M1	994521.2766
SL-S1M2	1083351.648
SL-S1T	1072569.444
SL-S2B	957472.5275
SL-S2M	1085578.947
SL-S2T	531627.907
SL-S3B	973923.0769
SL-S3Br	749631.5789
SL-S3M	650800
SL-S3T	725361.4458

Table S2. Cell density estimates for all February 2020 samples.

References

Ellis, B., P. Haaland, F. Hahne, N. Le Meur, N. Gopalakrishnan, J. Spidlen, M. Jiang, and G. Finak (2009), flowCore: Basic structures for flow cytometry data, *R package version*, *1*(0).

Klempay, B., N. Arandia-Gorostidi, A. E. Dekas, D. H. Bartlett, C. E. Carr, P. T. Doran, A. Dutta, N. Erazo, L. A. Fisher, and J. B. Glass (2021), Microbial diversity and activity in Southern California salterns and bitterns: analogues for remnant ocean worlds, *Environmental Microbiology*.

Webb, S. J., T. Rabsatt, N. Erazo, J. S. Bowman, and T. Barkay (2019), Impacts of Zostera eelgrasses on microbial community structure in San Diego coastal waters, *Elementa: Science of the Anthropocene*, *7*.